Work Package 1: Dynamical and Chemical Coupling between Stratosphere and Troposphere

Summary

The focus of this work package (WP1) was the analysis of inter-annual changes of ozone and temperature both in observations and model runs. Of particular interest were connections between stratospheric and tropospheric changes. Major achievements within WP1 were

- Preparation, testing and application of two versions of the chemistry-climate model ECHAM-4 / CHEM with full interaction between chemical species and model radiative transfer. The two 39 level versions were: E39/C, run by DLR-Oberpfaffenhofen. This version represents the atmosphere from surface to about 30 km altitude (1000 hPa to 10 hPa) and is called ECHAM-DLR in the following. The other version MAECHAM4/ CHEM, run by MPI Main/Hamburg, reaches from the surface to about 80 km (1000 hPa to 0.1 hPa). It is called ECHAM-MPI in the following. Both models represent the state-of-the-art in chemistry-climate modelling.
- Several multi-year simulations, among them 40-year transient runs (1960 to 1999) accounting for most known influences on the atmosphere, i.e. the anthropogenic increases of CO_2, chlorofluorocarbons (CFCs) and other source gases, the quasi-biennial oscillation of equatorial winds (QBO), historic sea-surface temperatures, volcanic aerosols and the 11-year solar cycle, by both ECHAM-DLR and ECHAM-MPI. Particularly the inclusion of the QBO and the realistic results for the 11-year solar cycle put these simulations into the international top tier.
- An in depth analysis of inter-annual variations of ozone and temperature from the longest available data sets for stratospheric ozone (and temperature) in particular from ozone-sondes and ground-based Laser Radars (lidars), but also from TOMS/SBUV satellite measurements and NCEP reanalyses.
- The most comprehensive comparison of the major sources of variability, both in observations and long-term transient model simulations. The simulations reproduce extremely well most characteristics of the observed annual cycle and of the observed inter-annual and long-term variations in ozone and temperature, i.e. long-term trends due to anthropogenically increasing chlorine, CO_2, and other source gases, and fluctuations related to QBO, 11-year solar-cycle, the strength of the polar winter vortices, tropospheric weather, El-Niño, and volcanic aerosol. Some model shortcomings are found in the strength and longitudinal distribution of the polar vortices. However, the achieved status of the ECHAM4/CHEM model and the thorough validation by long-term measurements are a major step forward.
- Lidar observations and analysis of various data sets on the question, whether the constant ozone levels observed in the upper stratosphere in recent years are a first sign of a "beginning recovery of the ozone layer" or a consequence of the recent solar maximum. Given the shortness of available observations since 1980 only, and the possible interference between the major volcanic eruptions of 1982 and 1991 with the 11-year solar-cycle, this question cannot be answered yet. Observations are needed until at least 2010 to answer it.
- Some of the most detailed and comprehensive model simulations of evolution and effects of the volcanically enhanced stratospheric aerosol layer after the 1991 Mt. Pinatubo aerosol layer being performed by MPI-MAECHAM.
- A study by MPI-MAECHAM using ECHAM-MPI time-slice experiments indicating that stratospheric ozone loss and increasing CO_2 have lead to significant cooling and stabilisation of the Arctic winter vortex in March and April. This is relevant for Arctic ozone loss and seems to have contributed to the cold winters observed in the 1990s.
- One of the first modelling studies on atmospheric effects of the 11-year solar-cycle (by MPI-C and others) that gives a realistic magnitude of stratospheric ozone and temperature effects and that shows a distinct influence in the troposphere as well.
- Analyses of connections between stratospheric polar vortex strength, QBO, 11-year solar cycle and tropospheric temperatures, winds or surface pressure confirming a potential for using stratospheric predictors to improve the long-term forecasting of tropospheric weather.

- Results were published and are being published in about a dozen refereed journal articles, as well as numerous conference contributions.
- Last not least, a very good working co-operation was established between the German modelling and observational groups involved in WP1. These close ties would be an ideal basis for further investigations on the underlying processes and for the prediction of the future evolution of the stratospheric ozone layer under a changing climate.

Joint contribution of DWD, DLR, MPI-C and MPI-M

Variance analysis of long time-series of observations and chemistry-climate model simulations

Global Climatologies

For selected months, Figure WP1-1 shows the climatological distribution of total column ozone, observed by the TOMS and SBUV satellite instruments (Stolarski and Hollandsworth, 2003), and simulated by the ECHAM-MPI (1000 to 0.1 hPa, 0 to 80 km altitude) and ECHAM- DLR (1000 to 10 hPa, 0 to 30 km altitude) transient runs. The corresponding climatologies for lower stratospheric temperature at 50 hPa (approx. 22 km altitude) are compared with NCEP Reanalyses (Kistler et al., 2001) in Figure WP1-1. In general, both model reproduce the observed distributions of total ozone and lower stratospheric temperature very well (see also Austin et al., 2003). The overall zonal distribution, low

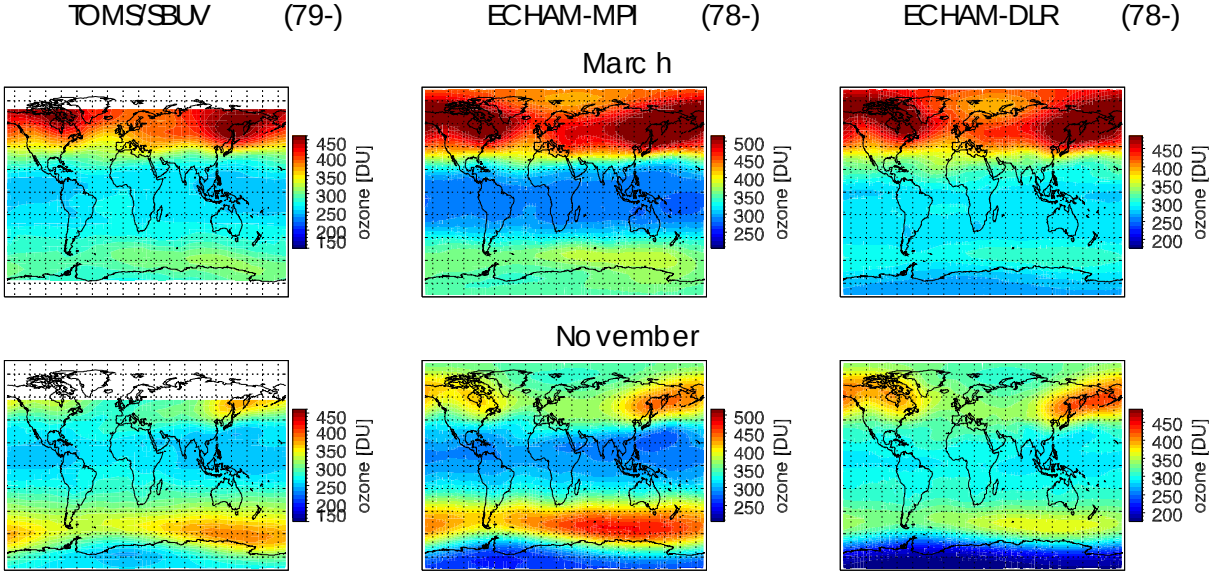

Figure WP1-1: Climatological distribution of total ozone. Left: SBUV/TOMS observations (1979 to 2002). Middle: ECHAM-MPI transient simulation (1978 to 1999). Right: ECHAM-DLR transient simulation (1978 to 1999).

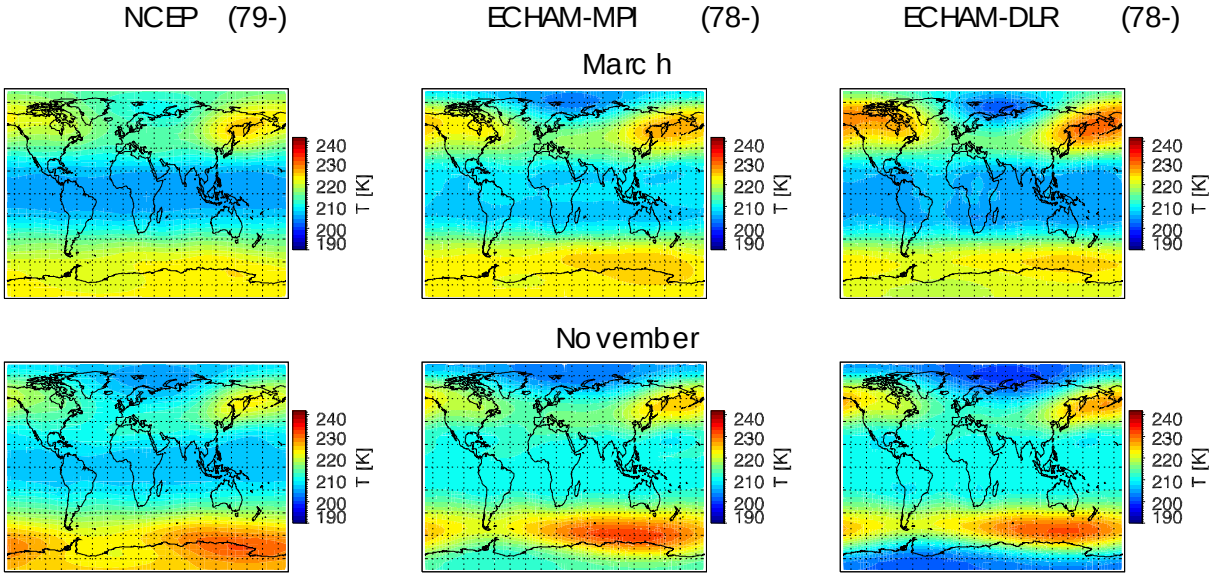

Figure WP1-2: Same as Fig. WP1-1, but for temperature at 50 hPa. Left: NCEP Reanalyses (1979 to 2002), Middle and Right: ECHAM model runs (1978 to 2002).

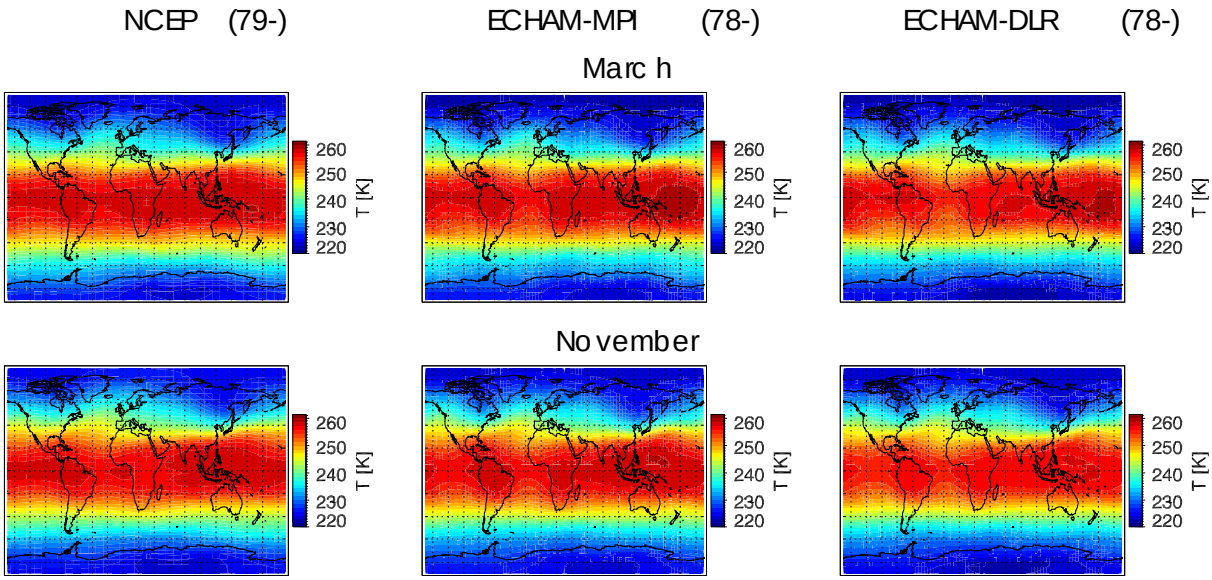

Figure WP1-3: Same as Fig. WP1-2, but for tropospheric temperature at 400 hPa.

values at low latitudes, high values at high latitudes, is reproduced well. The a-zonal Aleutian and Australian stratospheric anticyclones are also matched well. Both models tend to overestimate total ozone. This is very noticeable (100 DU) for ECHAM-MPI in the downward branch of the Brewer-Dobson Circulation at high latitudes. The higher total ozone is a result of numerical diffusion bringing ozone down too fast in the lower stratosphere (Steil et al., 2003). Because of the additional model levels around the tropopause, the effect is much reduced for ECHAM-DLR, albeit at the expense of model data missing above 30 km altitude. Both models exhibit the well known cold bias of the polar winter vortices. This is most pronounced for ECHAM-DLR over Antarctica.

For the troposphere and selected months, the distribution of temperature at 400 hPa (approx. 6 km altitude) is shown in Fig. WP1-3. Both model versions reproduce the observations very well. In particular, the land-sea contrast at northern mid-latitudes is matched successfully.

The variability encountered in observations and models and measured by the standard deviation of individual monthly means is compared in Figs. WP1-4 to WP1-6. As with the mean values, the models successfully reproduce most features of the observations. The highest variability is found near the

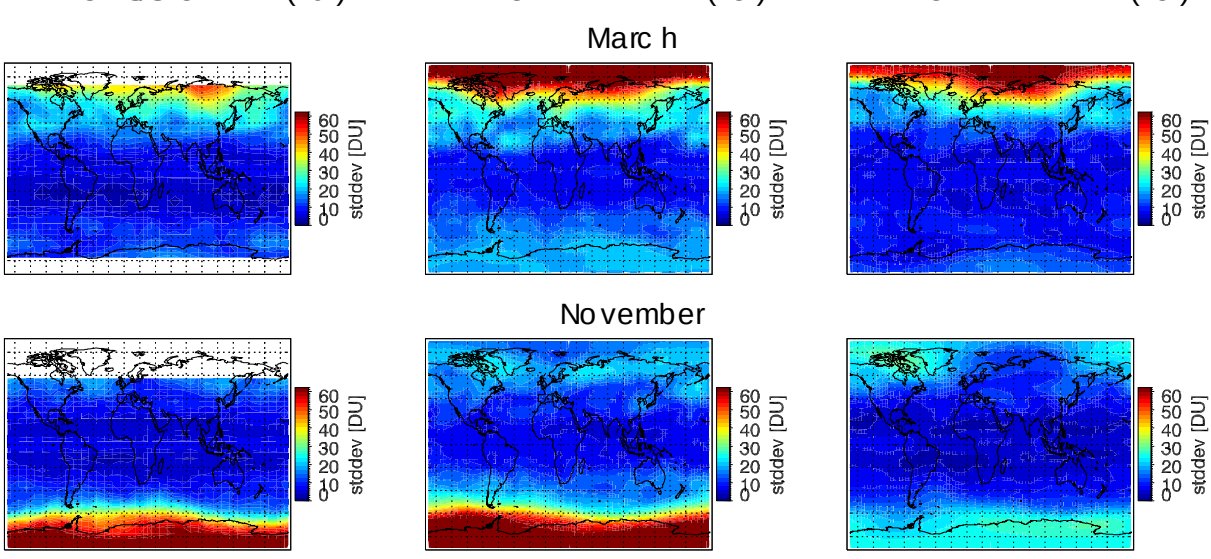

Figure WP1-4: Standard deviation of total ozone monthly means. Left: SBUV/TOMS observations (1979 to 2002). Middle ECHAM-MPI transient simulation (1978 to 1999). Right ECHAM-DLR transient simulation (1978 to 1999).

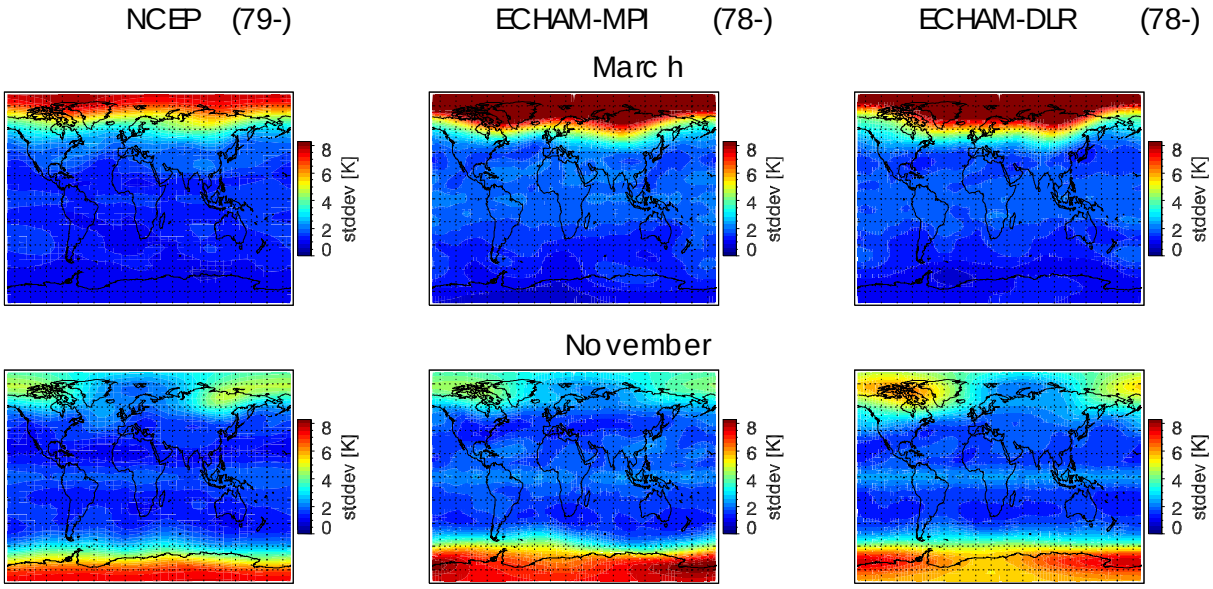

Figure WP1-5: Standard deviation of temperature monthly means at 50 hPa. Left: NCEP reanalyses (1979 to 2002). Middle ECHAM-MPI transient simulation (1978 to 1999). Right ECHAM-DLR transient simulation (1978 to 1999).

poles in winter and spring. Variability is lowest in the tropics, with a slight enhancement near the Equator. The latter is due to the QBO. A-zonal features at higher latitudes are seen in observations and models. However, the exact shape and location of these features tends to differ between observations and model runs. A general shortcoming of the models is the late break-up of the winter polar vortices, particularly of the Antarctic vortex for ECHAM-DLR. This means that at high latitudes the models show higher than observed variability in late spring and early summer. The too strong vortex in the models also tends to result in too low variability in the early half of winter, again particularly for the Antarctic vortex in ECHAM-DLR.

Tropospheric temperature presents a more complex behaviour. Again many general features of the observed distribution are reproduced by the model simulations. But Fig. WP1-6 also shows some differences.

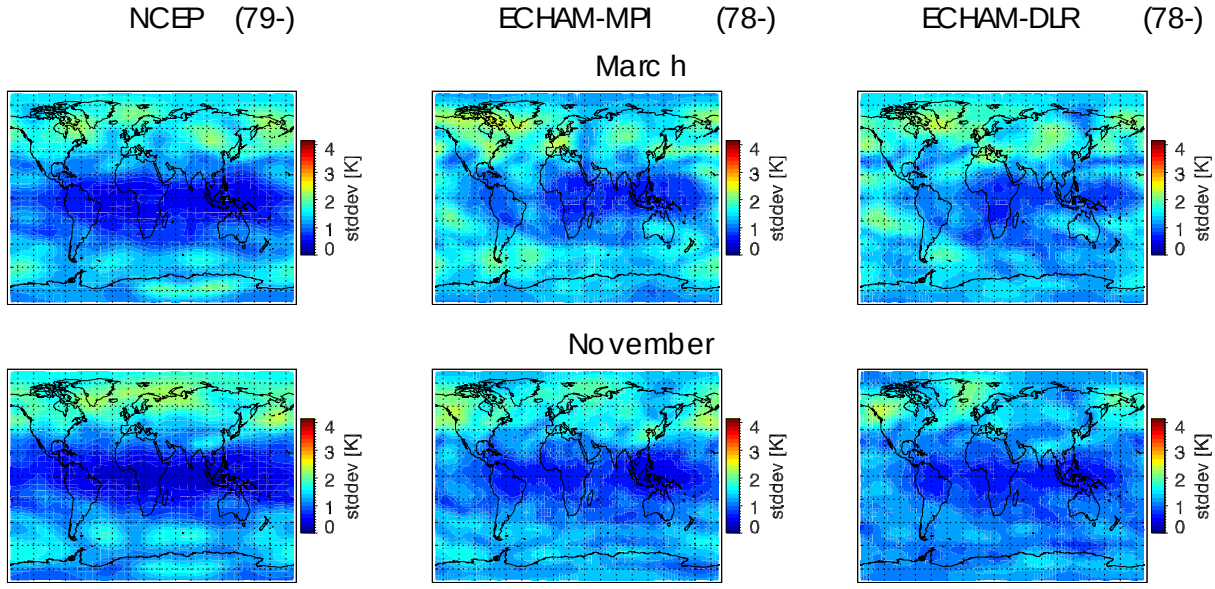

Figure WP1-6: Same as Fig. WP1-5, but for temperature at 400 hPa.

Multiple linear regression analysis of observed and modelled variations

A major task of this work package was the characterisation of various influences, such as long-term trend, 11-year solar cycle, quasi-biennial oscillation, etc. on observed and modelled ozone and temperature variations on monthly to decadal time-scales. Detection and quantification of these influences is a prerequisite for any further analysis of possible interactions. The characterisation was achieved by multiple linear regression analysis. A given deseasonalized ozone or temperature time series (left side of Eq. 1) is described as a linear combination of predictor-time series (right side of Eq. 1). The predictor time series are chosen a-priori to represent the main known influences on stratospheric ozone and temperature. After substantial testing the chosen predictors were: A linear trend term which largely represents the anthropogenic influence through increasing CFCs and greenhouse gases; a term representing the 11-year solar cycle; stratospheric aerosol optical depth as a descriptor of stratospheric aerosol loading, effective only after the eruptions of Agung (1963), El Chichon (1982) and Pinatubo (1991); equatorial zonal wind anomalies as a descriptor for the QBO (two orthogonal terms allow for proper phase-lag); tropospheric temperature anomalies at 400 hPa as a descriptor of tropospheric meteorological influences on the stratosphere; zonal wind anomalies at 60°N and 60°S as descriptors of the strength of the polar winter vortices; and, finally, a term representing the El-Niño Southern Oscillation.

$$\Delta O_3 = j*\text{lin.\_trend} + f*\text{solar\_cyle} + a*\text{strat.\_aerosol} + q_{10}*\text{QBO}_{10mb} + q_{30}*\text{QBO}_{30mb} + t*\text{dT\_400} + \text{w\_s}*\text{wind\_60S} + \text{w\_n}*\text{wind\_60N} + e*\text{ENSO} + \text{rest}$$

(**Eq. 1**)

For given ozone (or temperature-) anomalies and given predictor time series, the coefficients (j, f, a, q_{30}, q_{30}, ...) are determined through a least squares fitting procedure. In order to account for important influences only, predictors not significant at the 90% level were left out in a stepwise approach. This stepwise multiple regression was carried out separately for each grid cell of the global time-varying fields provided by SBUV/TOMS observations, NCEP reanalyses and the ECHAM-MPI and ECHAM-DLR transient simulations.

Figure WP1-7 shows the R^2 achieved when regressing observed or modelled ozone and 50 hPa temperature variations against the predictor time series. Here only data from the winter months December

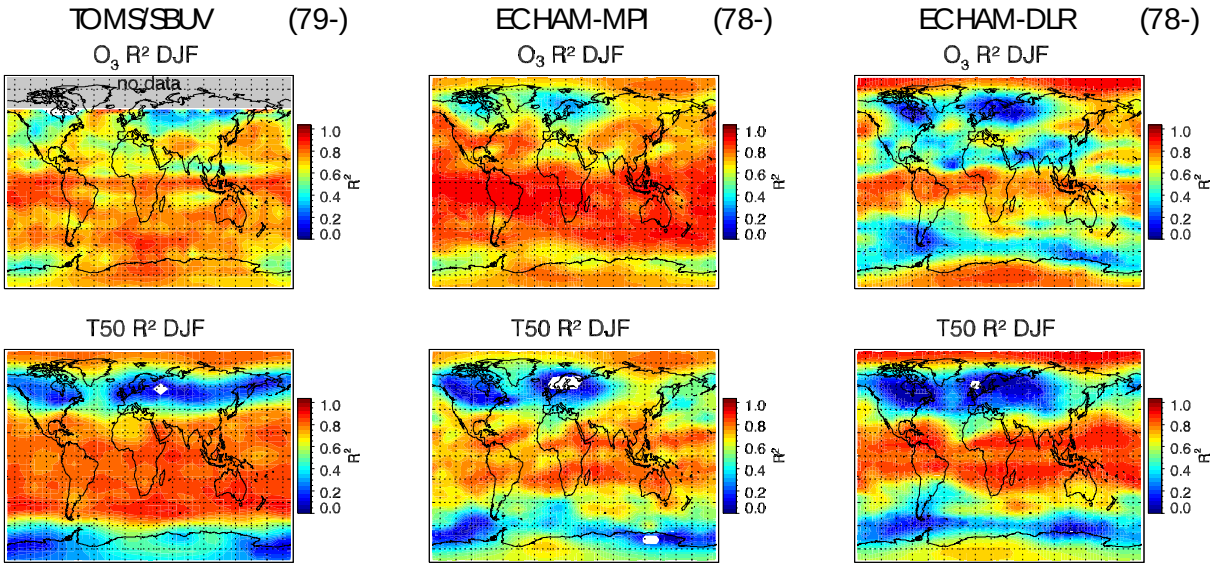

Figure WP1-7: Global distribution of R^2 obtained by multiple linear regression according to Eq. 1, for total ozone anomalies (upper rows) and temperature anomalies at 50 hPa (lower rows). Left: TOMS/SBUV observations and NCEP reanalyses. Middle: ECHAM-MPI simulation. Right: ECHAM-DLR simulation. Only data from the months December to February were used for this plot.

to February were used. R^2 is given by the ratio between the total variance of the left side term of Eq. 1, to the variance described by the regression, i.e. the variance of all terms on the right side of Eq. 1, except for the rest. A perfect regression would give R^2=1, i.e. the regression completely reproduces the observations on the left side of Eq. 1. Small $R^2 \approx 0$ indicates poor regression, reproducing only a small fraction of the observed variance. Small R^2 can either indicate that important predictors are missing, or that the data are inherently very noisy. Such noise cannot be reproduced by the usual predictors.

As indicated by the large red areas of high R^2 in Figure WP1-7, the regression is able to provide a very good reproduction of the observed and modelled total ozone variations over large areas of the globe, particularly in the tropics and near the poles. The regression works best for observed 50 hPa temperatures, or for ECHAM-MPI simulated total ozone. It works less well for ECHAM-DLR simulated total ozone. However, at northern and southern mid-latitudes substantial blue bands of poor regression are found, especially for 50 hPa temperature. At this point, it is not clear weather important predictors, e.g. accounting for the size and position of polar vortex, jet stream, or polar front are missing, or whether the poor regression is caused by chaotic noisy behaviour of the atmosphere in these regions. In areas with poor regression, the results following need to be interpreted with care.

The size of the linear trend terms obtained in the regression is given in Figure WP1-8. Both models reproduce the main features of the observed total ozone and 50 hPa temperature trends. The total ozone decline is largest at high latitudes and in winter, that is in the coldest regions of the atmosphere (compare Fig. WP1-2). While the model simulations reproduce the main features, the magnitude of the ozone decline appears to be overestimated by ECHAM-MPI and underestimated by ECHAM-DLR. ECHAM-DLR also shows slightly less stratospheric cooling than ECHAM-MPI or NCEP Reanalyses. The geographical distribution, significant cooling from the tropics up to mid-latitudes, but no significant cooling at high-latitudes, is quite similar for models and reanalyses. The total ozone and temperature trends found in this study are consistent with other investigations (e.g., Fioletov et al., 2003; Ramaswamy et al., 2001; WMO, 2003). The ozone decline must largely be attributed to chemical ozone destruction by anthropogenic chlorine and bromine. The lower stratospheric cooling is a consequence of decreasing ozone, which generally cools the stratosphere, increasing carbon dioxide, which cools the stratosphere, and changing water vapour (Shine et al., 2003).

Magnitude and distribution of total ozone and lower stratospheric temperature variations attributed to the QBO are shown in Figure WP1-9. As found in previous studies and summarised by Baldwin et al. (2001), the vertical wind shear associated with the QBO induces a meridional residual circulation with a descending branch in the tropics, below the westerly wind maximum, and an ascending branch in the

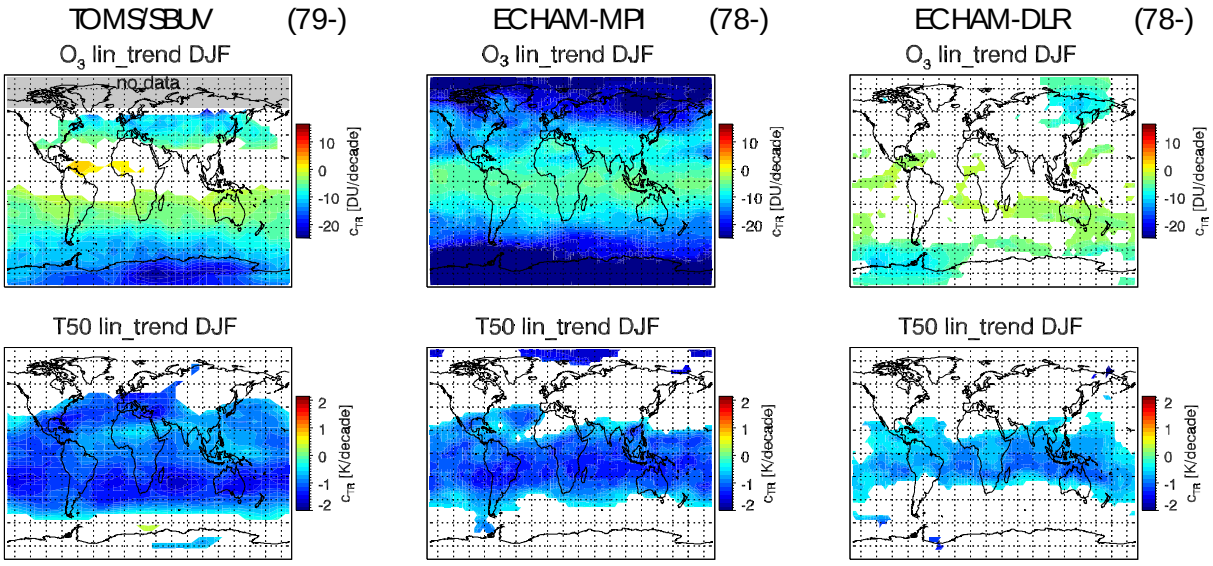

Figure WP1-8: Size of the linear trend for total ozone (top panels) and 50 hPa temperature (bottom panels), for observations (left), ECHAM-MPI simulation (middle) and ECHAM-DLR simulation (right). In the white areas the linear trend term was not statistically significant at the 90% confidence level.

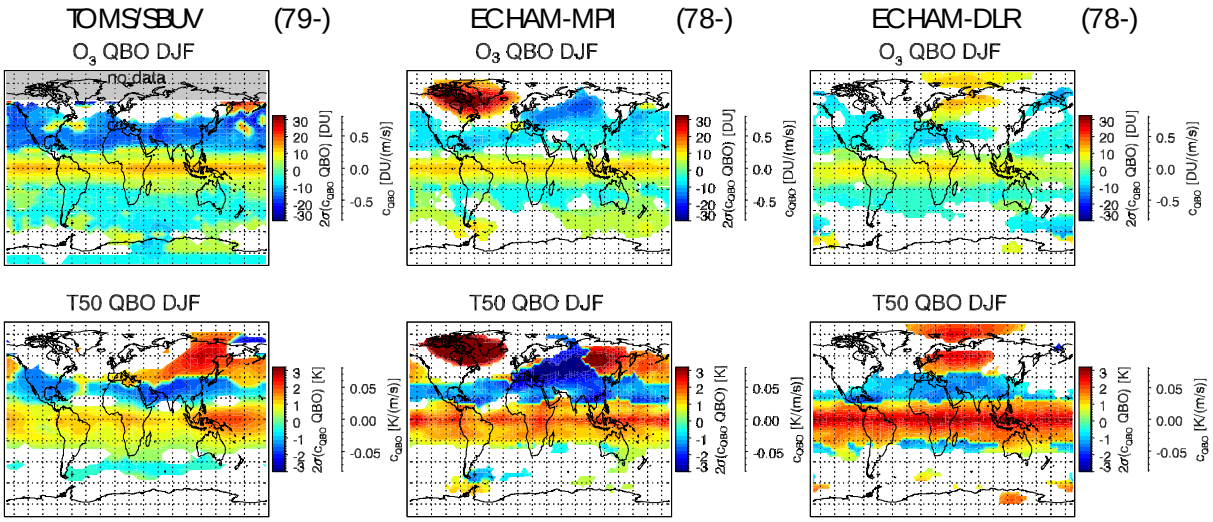

Figure WP1-9: Typical size of total ozone and 50 hPa temperature fluctuations that are attributed to the QBO. Plotted are 2 standard deviations of the QBO related time series terms in Eq. 1. Red colours indicate positive correlation of ozone or temperature anomaly with westerly wind anomalies at 30 hPa, blue colours indicate negative correlation. In the white regions, no statistically significant QBO influence is found (90% confidence level).

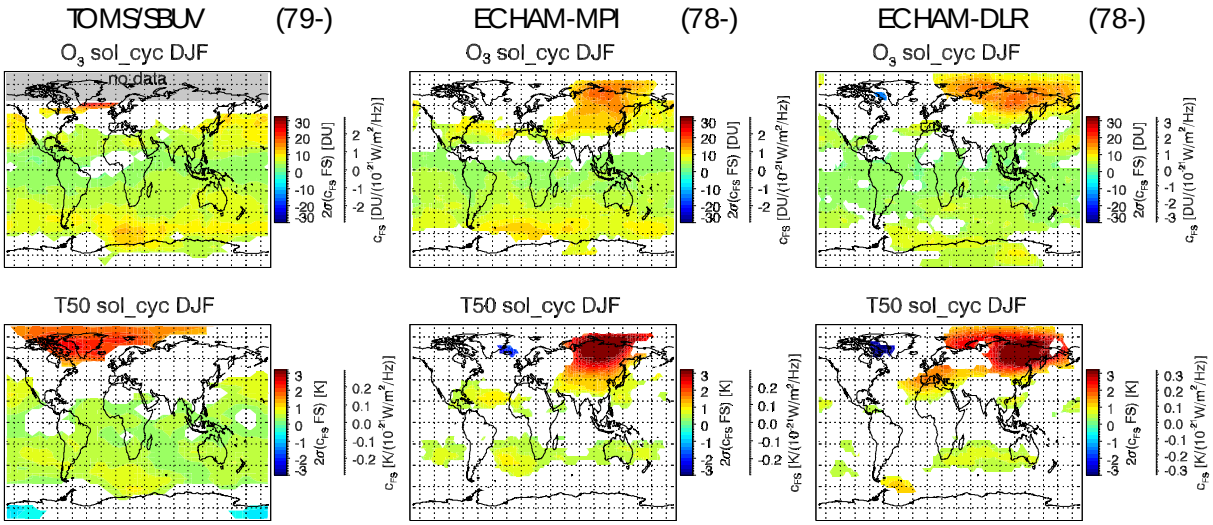

Figure WP1-10: Same as previous Figure, but for variations attributed to the 11-year solar-cycle.

extra-tropics. This brings ozone rich air down in the tropics and leads to adiabatic warming there. The ascending branch in the extra-tropics brings up ozone poor air and adiabatic cooling. Correspondingly, Fig. WP1-9 shows a tropical band of enhanced total ozone and 50 hPa temperatures, whereas both are lower in the extratropics (blue region). The extratropical effect is strongest in the winter hemisphere. At higher latitudes the zonal symmetry is broken. There observations and models show localised centres of high positive anomalies which are roughly in phase with the tropical anomaly. However, the longitude of these anomalies differs between observations and models. The observations show a positive anomaly west of the Aleutian High, whereas ECHAM-MPI shows a strong anomaly east of the Aleutian High, over Canada, and ECHAM–DLR shows an anomaly over Europe and Russia. Note the remarkable symmetry between total ozone and 50 hPa temperature, both in observations and model simulations.

Ozone and temperature variations attributed to the 11-year solar cycle are shown in Fig. WP1-10. As before, total ozone and 50 hPa temperature show very similar geographic distributions. Interestingly, the largest responses to the 11-year solar cycle are found near the winter pole, where solar irradiation is smallest. A broad region of enhanced ozone and temperature reaches from southern to the northern

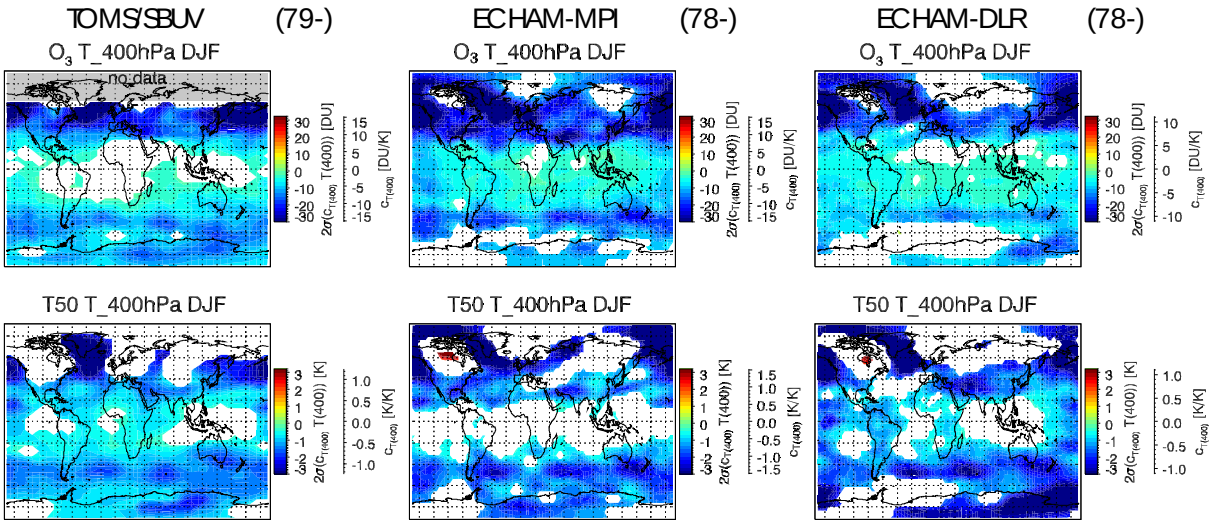

Figure WP1-11: Same as previous Figures, but showing the size of variations associated with anomalies of tropospheric temperature at 400 hPa.

mid-latitudes. The model simulations reproduce the ozone signal quite well. The modelled temperature response is slightly smaller. As with the QBO there is a very large, zonally asymmetric response at high latitudes. The models also produce such a structure, however, at a different location than observations and reanalyses.

An important influence on total ozone and lower stratospheric temperature comes from tropospheric weather systems. Tropospheric cyclones have rising motions in the troposphere which are compensated by sinking motion in the lower stratosphere. There is also advection of low-latitude or high latitude air-masses in the different sectors of a tropospheric cyclone, reaching up into the stratosphere (Koch et al., 2003). A simplified way of accounting for such variations is to use temperature anomalies e.g. at 400 hPa (or tropopause height) as one predictor in Eq. 1. Figure WP1-11 shows the typical size of ozone and 50 hPa temperature variations associated with changes in tropospheric temperature at 400 hPa. One of the findings of this study was that tropopause height and 400 hPa temperature are roughly equivalent as predictors. Both worked better than more complex predictors, e.g. circulation indices describing how pronounced given empirical circulation patterns (EOFs) are in a given month. As Figure WP1-11 shows, both models very closely reproduce the observed influence of 400 hPa temperature. In particular there is almost no difference between ECHAM-MPI, which has fewer model-levels near the tropopause, and ECHAM-DLR with many levels near the tropopause.

The largest variability of the lower stratosphere occurs in winter near the pole. It is associated with the

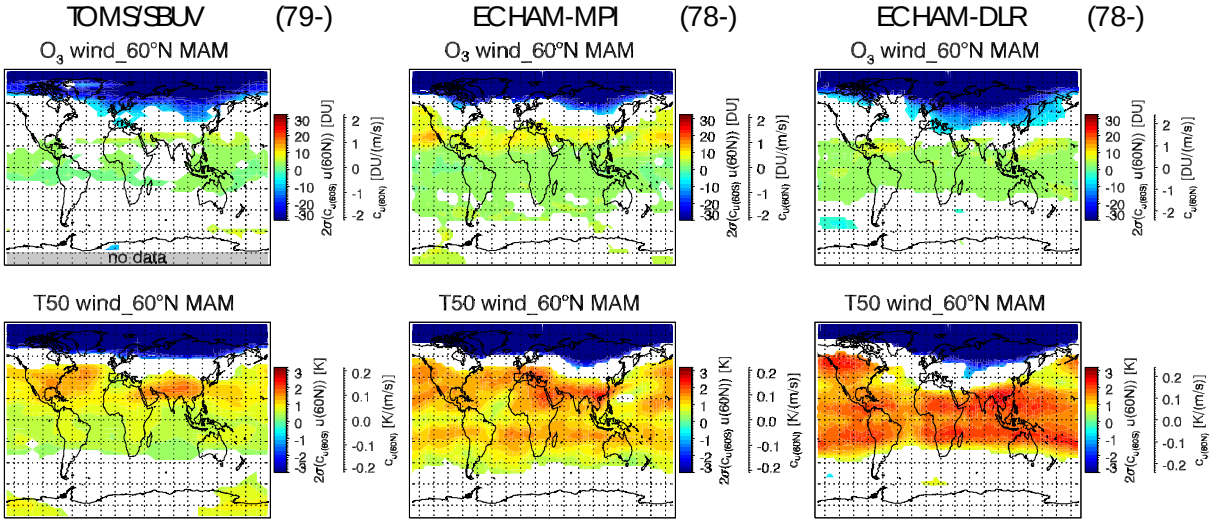

Figure WP1-12: Same as previous Figures, but for northern spring (March, April, May), and variations associated with zonal wind anomalies at 60°N, 50 hPa.

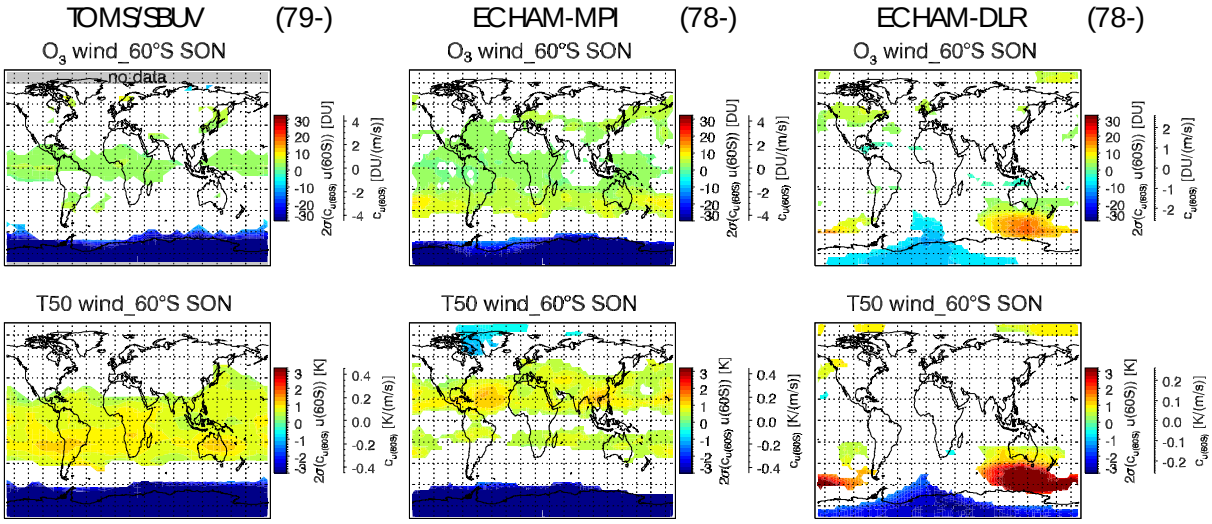

Figure WP1-13: Same as previous Figures, but for southern spring (September, October, November), and variations associated with zonal wind anomalies at 60°S, 50 hPa.

strength of the polar winter vortices. A strong vortex means low polar temperatures, due to isolation from lower latitudes, missing solar irradiation and diabatic cooling. Total ozone is then also low, due to reduced transport of ozone rich air from lower latitudes and due to enhanced chemical destruction of ozone by lower temperature, in particular if the low temperatures lead to polar stratospheric clouds. A weak vortex, on the other hand has usually been caused by stratospheric warmings bringing warm, ozone rich air to the pole. The substantial ozone and temperature variations that are connected with polar vortex strength are shown in Figs. WP1-12 and WP1-13. In Eq. 1, zonal wind anomalies at 60° latitude and 30 hPa pressure altitude are used a proxy for the strength of the polar vortex. High westerly winds are associated with a strong, well established vortex, whereas low westerly or easterly winds indicate that the vortex is weak and disturbed, or has broken down completely.

The expected patterns for total ozone and 50 hPa temperature variations can be seen in Figs. WP1-12 and WP1-13. Note that these results are for northern (MAM) and southern spring (SON), not northern winter (DJF) as in the other figures. A strong polar vortex, i.e. high zonal wind is clearly associated with low total ozone and cold temperatures in the polar cap, and enhanced total ozone and warm temperatures at lower latitudes. Due to reduced transport, less ozone is transported from low latitudes into the polar region. In addition, low temperatures enhance spring-time ozone depletion ("the ozone hole"). According to other studies (e.g., Rex et al., 2004) both transport and chemistry changes con-

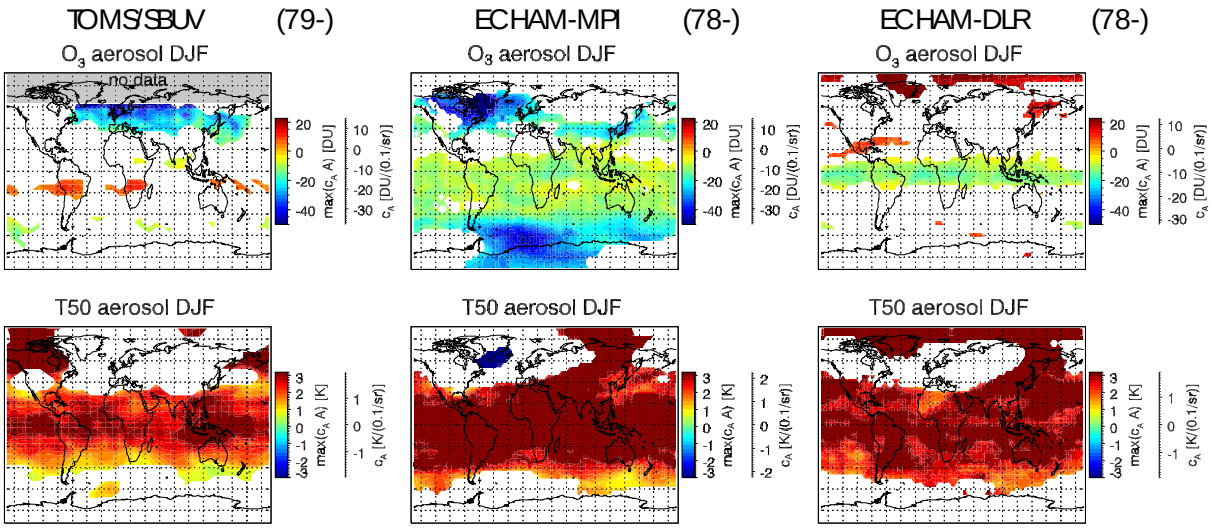

Figure WP1-14: Maximum changes of total ozone and 50 hPa temperature attributed to stratospheric volcanic aerosol after the eruption of Mt. Pinatubo in June 1991. In the white areas there was no significant aerosol effect at the 90% confidence level.

tribute about one half to the observed variations. A very similar picture is seen for temperatures at 50 hPa. A reduced Brewer Dobson circulation means less transport of warm air, and weaker downwelling and adiabatic warming in the polar region, as well as weaker upwelling and adiabatic cooling at low latitudes. The reduced (or enhanced) ozone also reduces (enhances) diabatic heating by long-wave radiation from below and short-wave radiation from above.

Most of the observed features are again reproduced quite well in the model simulations. However the latitudinal structure of the polar response is not always reproduced. ECHAM-DLR shows a different Antarctic response in Fig. WP1-13, likely because of the too cold and too long lasting Antarctic vortex in this model.

Fig. WP1-14 shows total ozone and 50 hPa temperature response to volcanically enhanced stratospheric aerosol. Note that this response largely represents anomalies found in the first year after the three volcanic eruptions of Agung (1963), El Chichon (1982) and Pinatubo (1991). Given the uncertainties of correctly accounting for all other influences in Eq. 1, the response to volcanic aerosol has to be interpreted with care.

Observations and models show substantial warming in a wide belt around the equator. At high latitudes an a-zonal signature is found again, which looks like an eastward extension of the Aleutian High in the observations, but like a westward extension in the simulations. Note that the warming is generally stronger in the simulations. For total ozone, observations and ECHAM-MPI show strong ozone depletion at northern latitudes, but less or no ozone depletion at low latitudes. ECHAM-MPI produces stronger and more widespread ozone depletion than observed. Contrary to observations and ECHAM-MPI, the ECHAM-DLR transient simulation has a stratospheric warming in the northern winter following Pinatubo. Therefore, it does not show high-latitude ozone depletion. Its aerosol signal, or lack of it, in the southern hemisphere is similar to the observations.

Note that stratospheric warmings occur largely by random both in reality and in realistic simulations. It cannot be expected that any given simulation will find warmings at the same time, and under the same conditions as observations, or another simulation. However, ECHAM-DLR has a tendency to produce more warmings than other models (Austin et al., 2003).

Substantial variability is associated with the El-Niño/ Southern Oscillation Phenomenon (ENSO). During the El-Niño warm-phase, ocean surface temperature in the Eastern Tropical Pacific is 1 to 2 K above normal, during the La-Niña cold-phase it is 1 to 2 K below normal. These changes are accompanied by changes in many atmospheric parameters, e.g. tropospheric winds and rainfall patterns. During El-Niño, tropical easterlies weaken, dry conditions are found in the Western Pacific (Australia, In-

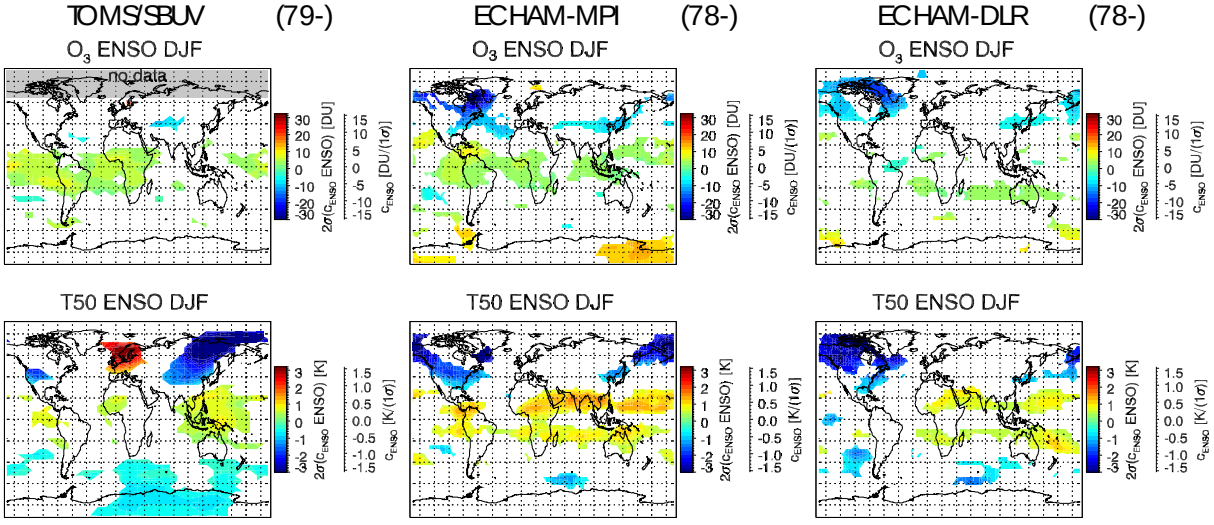

Figure WP1-15: Typical size (2 standard deviations) of total ozone and temperature fluctuations attributed to the Southern Oscillation index. This predictor is positive during La-Niña events and negative during El-Niño events.

donesia), wet conditions extend further into the Eastern Pacific (South America). The warmer sea surface temperatures also lead to a warmer troposphere and a higher tropopause, particularly over the Eastern Tropical Pacific. In the extra tropics, particularly over Eastern Asia and the Pacific, temperatures and tropopause height are lower. The opposite is the case for La-Niña. The tropospheric changes are compensated in the lower stratosphere.

Figure WP1-15 shows that total ozone and 50 hPa temperature are high during La-Niñas throughout parts of the tropics, particularly around the Pacific, and low during El-Niños. Outside of the tropics, total ozone and 50 hPa temperature are generally low during La-Niñas, and high during El-Niños. The observed distribution is reproduced reasonably well in the model simulations. ECHAM-MPI seems to have a higher ENSO signal than ECHAM-DLR. Note that ENSO and 400 hPa temperature are highly correlated over the Pacific. Therefore part of the ENSO signal is already accounted for by the 400 hPa temperature predictor. However, Fig. WP1-15 does not change substantially, when 400 hPa temperature is left out of the regression.

Again, a zonally asymmetric feature appears at northern high latitudes. Substantially colder 50 hPa temperatures, and generally lower total ozone are found during La-Niña. In the model runs this feature is found over North America, whereas the NCEP reanalyses show it over Eastern Asia. TOMS/SBUV data only show a small positive anomaly over Scandinavia, that is also present in the NCEP reanalyses, but not in the ECHAM runs. The temperature anomalies indicate a weakening of parts of the Aleutian anti-cyclone. This is likely related to a generally stronger and more stable Arctic polar vortex during La-Niña (Labitzke and van Loon, 1999).

Tropospheric Temperature

Most of the factors relevant for the stratosphere also have some relevance in the tropopsphere. Figure WP1-16 shows results for the regression of tropospheric temperature anomalies at 400 hPa. In the troposphere, R^2 (top row) is much smaller than typical R^2 for total ozone or lower stratospheric temperature. The given set of, primarily stratospheric, predictors does not account for a large fraction of tropospheric variance. Nevertheless, the regression accounts for a substantial fraction of the variance (large R^2) in the tropical belt, and in the Pacific region in particular. This is due to ENSO, the most important source of variance in this region, being accounted for in the regression.

The tropospheric ENSO effect is summarised in the 2nd row of Fig. WP1-16: During La-Niñas, the Southern Oscillation Index used as predictor is positive, sea surface temperatures are lower in the Eastern Pacific. This is reflected in lower tropospheric temperatures over the Pacific and the entire tropical belt (blue region in the figure). The lower tropical temperatures are compensated by warmer temperatures in certain regions of the extra-tropics (red and yellow in the figure). Modelled and observed ENSO effects are very similar.

As the 3rd and 4th row of Figure WP1-16 show, the strength of the polar vortices, represented by zonal wind anomalies at 60° and 30 hPa, also has a significant effect on tropospheric temperature. When the polar vortex is strong, lower temperatures are found in the polar troposphere, whereas tropospheric temperatures tend to be warmer over parts of the mid-latitudes. There are indications of an effect in the tropics as well. However the tropical connection seems to be different for northern and southern vortex. This connection between polar stratospheric vortex and the underlying troposphere is well known. It is often termed Arctic and Antarctic Oscillation (Perlwitz and Graf, 1995; Baldwin and Dunkerton, 1999). See also WP2 of this report. As the figure shows, both northern and southern connections are reproduced very well by the simulations.

Although the linear trend found in the NCEP analyses has to be regarded with suspicion because of substantial changes over time in the underlying observation systems, particularly in the southern hemisphere, there is quite a reasonable agreement between observed and modelled tropospheric warming.

Fairly small, but significant connections of tropospheric temperature to QBO and 11-year solar-cycle are found in the two lowermost rows of Fig. WP1-16. Solar maxima go hand in hand with enhanced temperatures in parts of the tropics and parts of the higher-latitudes, as well as lower temperatures in parts of the extra-tropics. Note that solar cycle and QBO effects that directly affect polar vortex strength, are already accounted for by that predictor (see also discussion of Fig. WP1-35). The QBO seems to be associated with banded structures in tropospheric temperature as well (c.f. Coughlin and Tung, 2001) For both solar-cycle, and QBO, agreement between the patchy observed and modelled signals is very encouraging.

Figure WP1-16 gives several examples for, albeit small, stratospheric connections to tropospheric temperature. The most important ones are the strength of the polar vortices, which have a distinct influence on tropospheric meteorology (Baldwin and Dunkerton, 1999). However, apart from affecting polar vortex strength directly, QBO and solar-cycle also show connections, both in observations and simulations. It is new and important, that both ECHAM simulations reproduce the observed connections. Since the stratospheric circulation changes on longer time-scales (up to years for QBO and solar-cycle), these connections may be useful for long-term weather forecasting. A more detailed analysis is certainly merited.

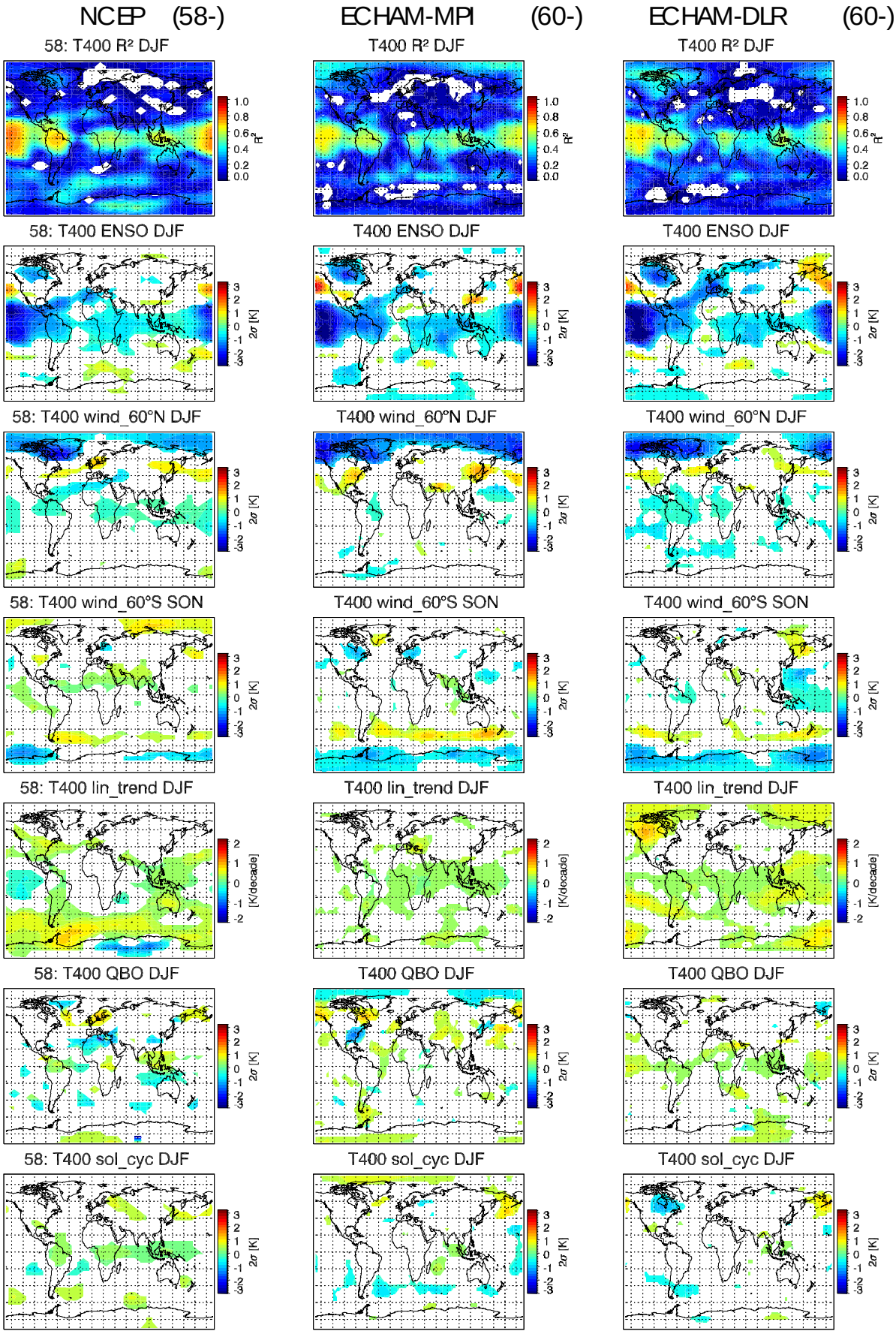

Figure WP1-16: Regression results for tropospheric 400 hPa temperature anomalies, showing the typical size (=2 standard deviations of corresponding terms in Eq. 1) of various predictors, as well as the R^2 (top row) for NCEP reanalyses since 1958, and ECHAM transient simulations since 1960.

Station data

A major achievement of this work-package was the analysis of ozone and temperature variations from long time series of ozone sounding and lidar stations. Data sources were the WOUDC and NDSC data bases. Figure WP1-17 shows the stations used. All these stations have regular high-quality ozone soundings over the last 20 to 40 years, and/or regular lidar measurements for at least 5 to 15 years. Note, that for Europe, not all possible stations were included in this study, because time series of stations like Payerne, Uccle, or Lindenberg are very similar to the Hohenpeissenberg time series.

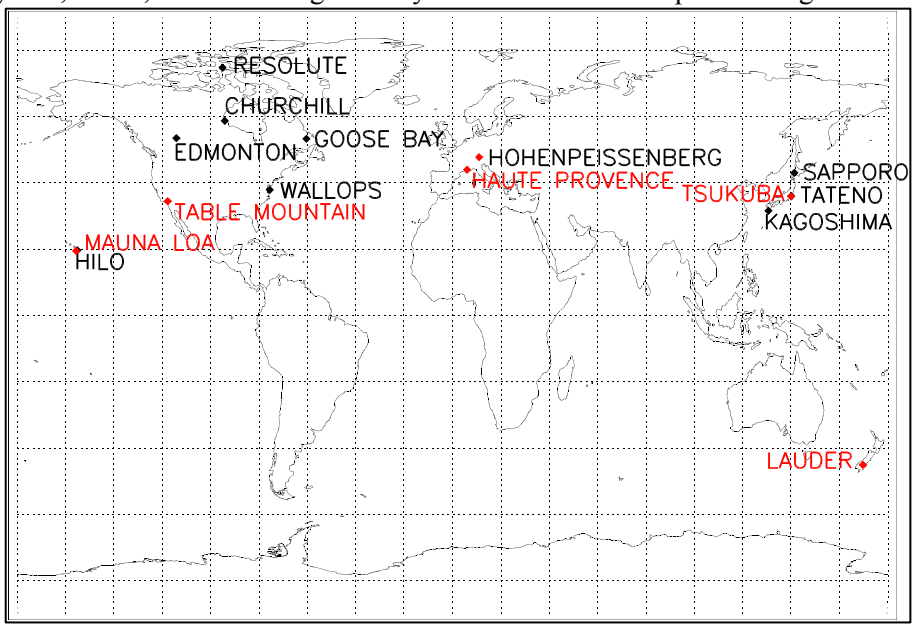

Figure WP1-17: Ozone-sonde (black) and lidar (red) stations used in this investigation.

Figure WP1-18 shows the ozone and temperature climatologies for a few of these stations. Ozone number density peaks somewhere between 15 and 25 km, at lower altitudes in the polar regions and at higher altitudes near the equator. Except for the tropics, the highest ozone densities are reached in the lower stratosphere in spring, the lowest in fall. This reflects the seasonal variation of the Brewer-Dobson Circulation, which brings ozone rich air down at higher latitudes in winter and fall. Upper stratospheric and tropical ozone peak in the summer, because photochemical ozone production follows solar irradiation and is strongest in summer. These components of the ozone annual cycle are most pronounced at high latitudes, and almost missing in the tropics. Depending on the station, tropospheric ozone peaks either in spring (most stations), due to high downward transport from the stratosphere, or in the summer (Hohenpeissenberg), due to photochemical production.

At higher latitudes, temperature at all altitudes peaks in the summer. Temperature maxima are found near the ground and at the stratopause near 50 km altitude. They reflect the maxima of heating from the ground and heating from stratospheric ozone peaking above the maximum of ozone mixing ratio, which occurs around 35 km altitude. Note that for Tateno/Tsukuba lower stratospheric temperature peaks in the winter. This is due to the downward motion and adiabatic heating induced by the Aleutian High. At Hilo, the temperature annual cycle is not very pronounced. Instead a clear signature of the semi-annual oscillation is visible in the upper stratosphere.

The two model simulations reproduce the observed ozone and temperature climatology quite well. As mentioned before, ECHAM-DLR and ECHAM-MPI in particular, tend to have too much ozone in the lower stratosphere due too much downward transport by numerical diffusion. As also mentioned, the polar vortex is generally too strong and lasts too long in the model simulations, particularly for ECHAM-DLR.

The climatological variability, measured by the standard deviation of all monthly means, is shown in Figure WP1-19. Note that the observed variability is often higher than the model results. This has to

be expected because measurement noise, sampling noise due to infrequent measurements, and small scale phenomena all increase the variability of observed monthly means, but are not present in the model simulations. Hohenpeissenberg, for example, has more frequent samples than most other stations. There, the standard deviations, particularly in the lower stratosphere, are smaller and more similar to the model simulations.

For ozone, the highest (relative) variability occurs near the tropopause and in the lower stratosphere, and in spring. Very low ozone variability is found in the mid-stratosphere and in summer. Temperature variability is highest, by far, throughout the stratosphere in winter and spring. This high variability is due to the highly variable polar winter vortex, which often breaks down due to stratospheric warmings. Thus winter variability is most pronounced at the high latitude stations. Temperature variability is very low in the stratosphere in summer and in the tropics. The tropopause region exhibits particularly low temperature variations and appears in Fig. WP1-19 as a dark band throughout the year in observations and simulations.

An interesting features is the high ozone variability in the troposphere in summer for Tsukuba/Tateno, both in observations and simulations. Noise limitations of the measurements can be seen for Hohenpeissenberg at the highest shown altitudes, or in tropospheric ozone variability at Hilo. Interesting is also the high temperature variability seen at Hohenpeissenberg in October, both in troposphere and upper stratosphere, or at Tsukuba in September.

Apart from the above mentioned difference in magnitude, the general structures of observed and modelled monthly mean standard deviations are very similar for observations and simulations. One of the differences is that variability related to the polar winter vortex lasts longer into spring in the simulations than in the observations, e.g. at Resolute. This effect of the “cold pole bias” has been discussed before.

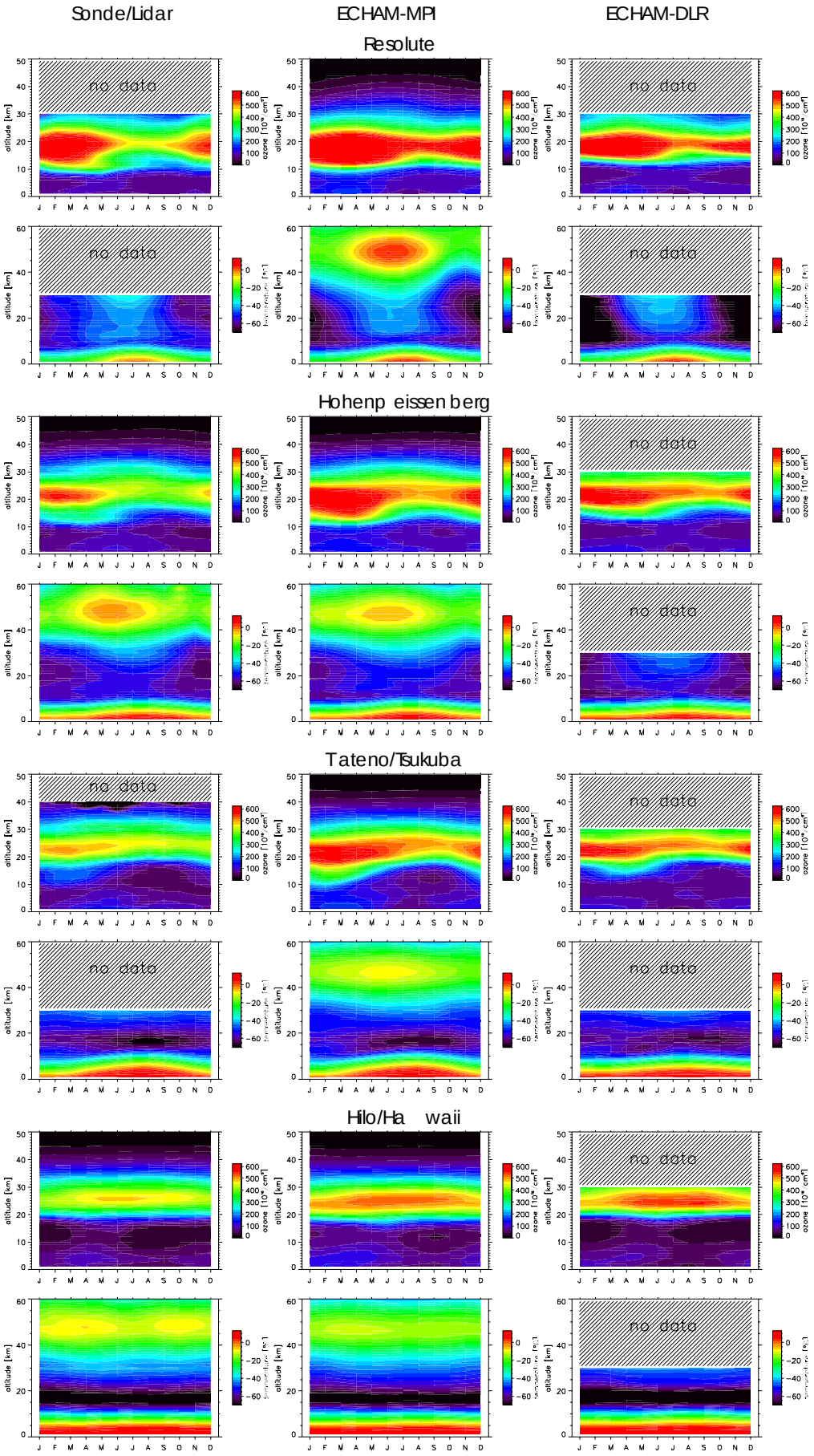

Figure WP1-18: Climatological ozone number density (upper rows) and temperature (lower rows) as a function of month of the year and altitude for selected stations. Left: Observations. Middle: ECHAM-MPI transient simulation. Right: ECHAM-DLR transient simulation.

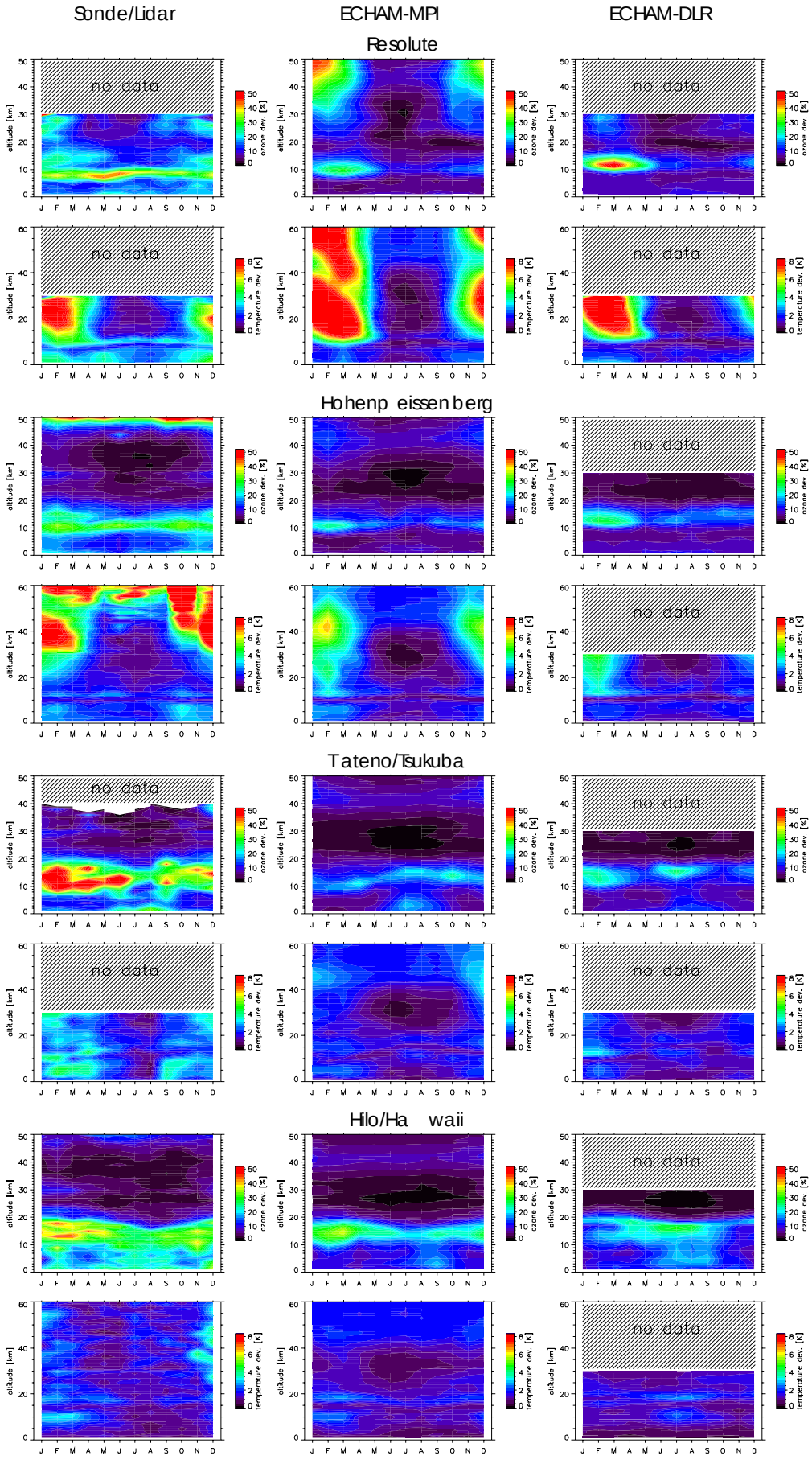

Figure WP1-19: Standard-deviation of individual monthly means from the long-term mean, for selected stations. First rows Relative standard deviation of ozone density, second rows Temperature standard deviation. Left: Observations. Middle: ECHAM-MPI transient simulation. Right: ECHAM-DLR transient simulation.

Regression Analysis for Station Data

Regression analysis following Eq. 1 was also performed for the station data. Note that above 30 km, temperature anomalies were introduced as an additional predictor for ozone and ozone anomalies were introduced as an additional predictor for temperature. Also, for the observations, tropopause height anomalies were used instead of 400 hPa temperature anomalies as the predictor accounting for tropospheric meteorological conditions. Finally, to be compatible with the lidar observations, only data after 1987 were used above 30 km for the model simulations. Note that the latter restriction does not have a large effect. Very similar results are obtained when simulation data since 1960 are included.

Figures WP1-20 to WP1-28 summarise the regression results for a few selected stations. As expected from the higher standard deviations due to measurement and sampling noise, R^2 is generally lower for the observations than for the model simulations. In the upper stratosphere, a very large fraction of the variance from the ECHAM-MPI simulation can be accounted for by the regression analysis. The regression also works reasonably well in the lowermost stratosphere, but results are generally poor in the mid-stratosphere. To a large degree this is due to the very low variance occurring in this part of the atmosphere. Particularly for temperature, the regression works well in the troposphere. This is no surprise as either the tropopause height or the 400 hPa temperature predictor are more or less identical to tropospheric temperature fluctuations.

For the selected stations, Fig. WP1-21 shows the linear trends obtained for ozone and temperature as a function of season and altitude. The most prominent feature is the large ozone decline at the higher latitude stations in the upper stratosphere, both in observations and ECHAM-MPI simulation. ECHAM-MPI also shows large cooling in the extra-tropical upper stratosphere. However, so far this cooling is not confirmed by the lidar data. Observations and simulations do show substantial ozone depletion and substantial cooling in the lower stratosphere. There is general agreement between observations and simulations that tropospheric ozone has been increasing.

Figure WP1-22 shows the size (=2 standard deviation of the corresponding terms on the right side of Eq. 1) of QBO related ozone and temperature variations. The picture is quite complex, with changes from positive to negative correlation with equatorial winds at 30 hPa occurring between seasons and between different altitudes. QBO related ozone and temperature fluctuations can be quite large and often exceed 10% or 4 K. In general there is reasonable agreement between observations and simulation. The QBO signal is significant over a wider altitude range and over more seasons for the simulations. Both simulations show very similar results. In ECHAM-MPI, the QBO signal in ozone seems to propagate too much into the troposphere.

Sizes of ozone and temperature fluctuations attributed to the 11-year solar cycle are shown in Fig. WP1-23. Ozone and temperature are higher in the upper stratosphere during solar maxima. This has to be expected since enhanced UV radiation during solar maxima should also lead to more ozone production in the upper stratosphere. The solar cycle effect seems to be largest at mid-latitudes, and more patchy at Hilo and Resolute. The agreement between observations and simulations is often poor. (See contribution from MPI-C below for more details).

The ozone and temperature fluctuations attributed to tropopause height (observations) or 400 hPa temperature anomalies (ECHAM simulations) from Fig. WP1-24 are very similar for observations and simulations. As expected the lower stratosphere is affected the most. There, ozone and temperature are low when the tropopause is high, or the troposphere is warm.

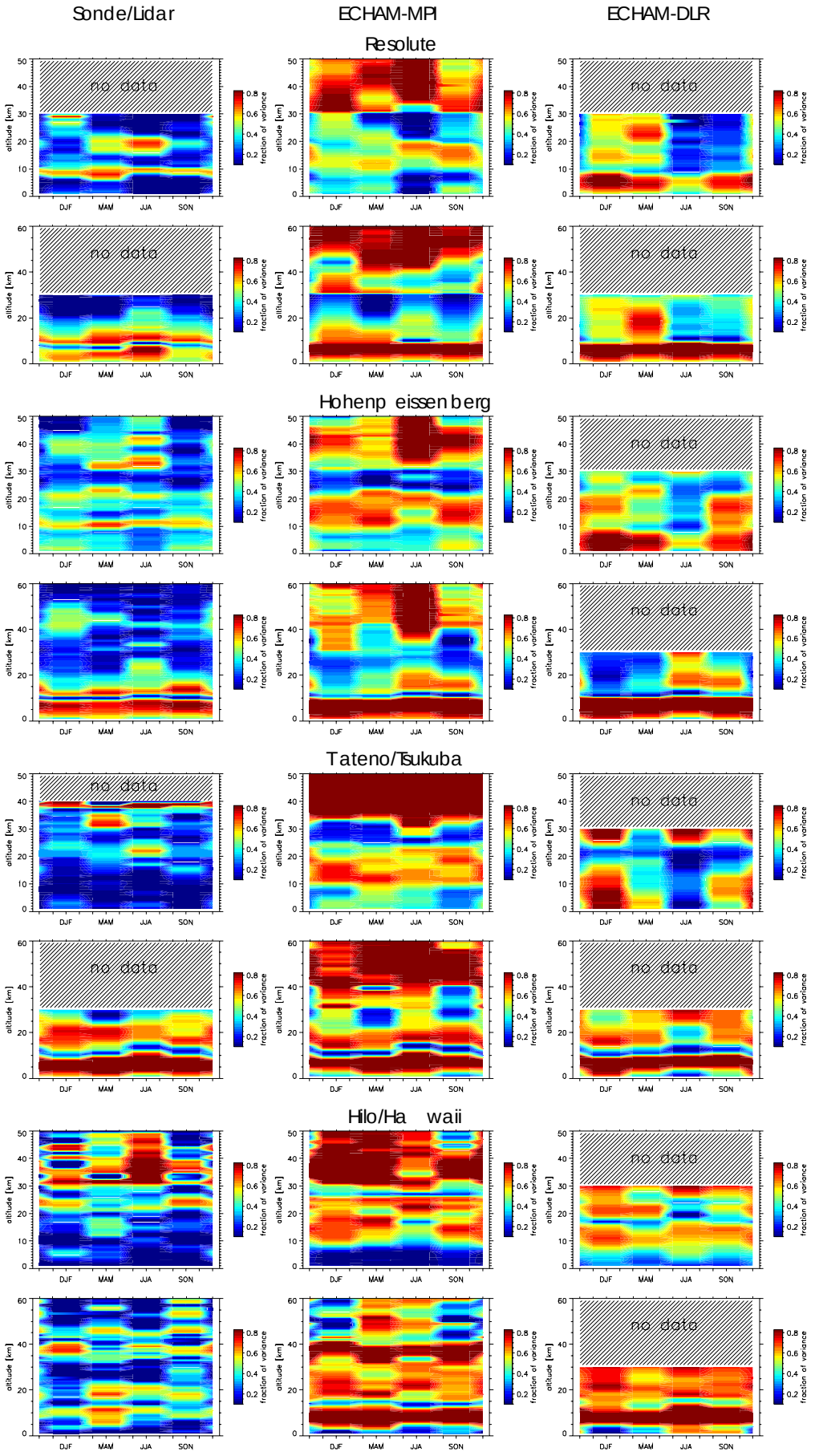

Figure WP1-20: R^2 of multiple linear regression according to Eq. 1 versus season and altitude. Upper rows: Ozone anomalies. Lower rows: Temperature anomalies at 50 hPa (lower rows). Left: Sondes (below 30 km) and lidars (above 30 km). Middle: ECHAM-MPI. Right: ECHAM-DLR.

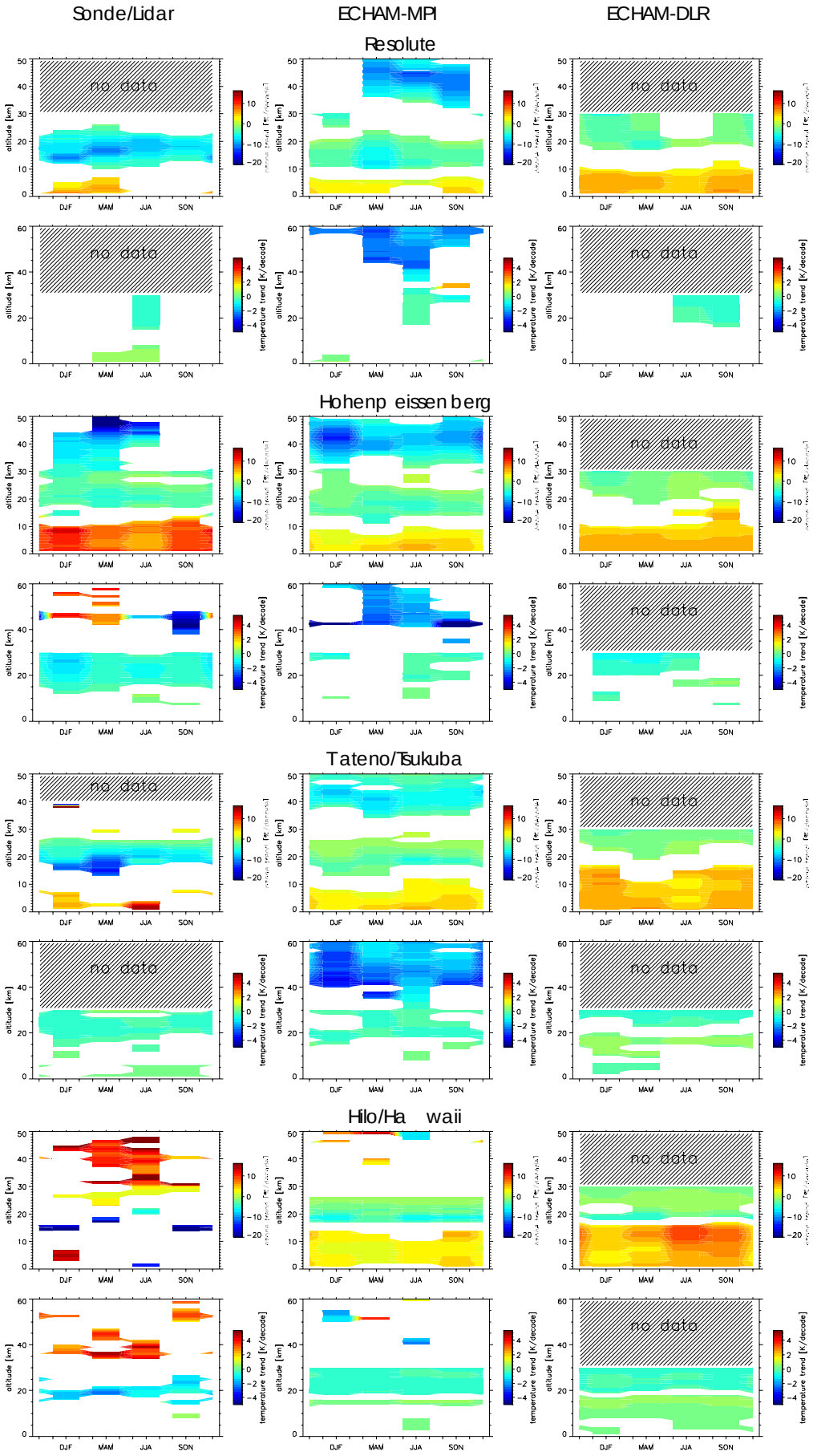

Figure WP1-21: Linear trend for ozone (upper rows) and temperature (lower rows) as a function of season and altitude, for combined sonde and lidar observations (left), ECHAM-MPI (middle) and ECHAM-DLR (right). In the white areas the linear trend term was not statistically significant at the 90% confidence level.

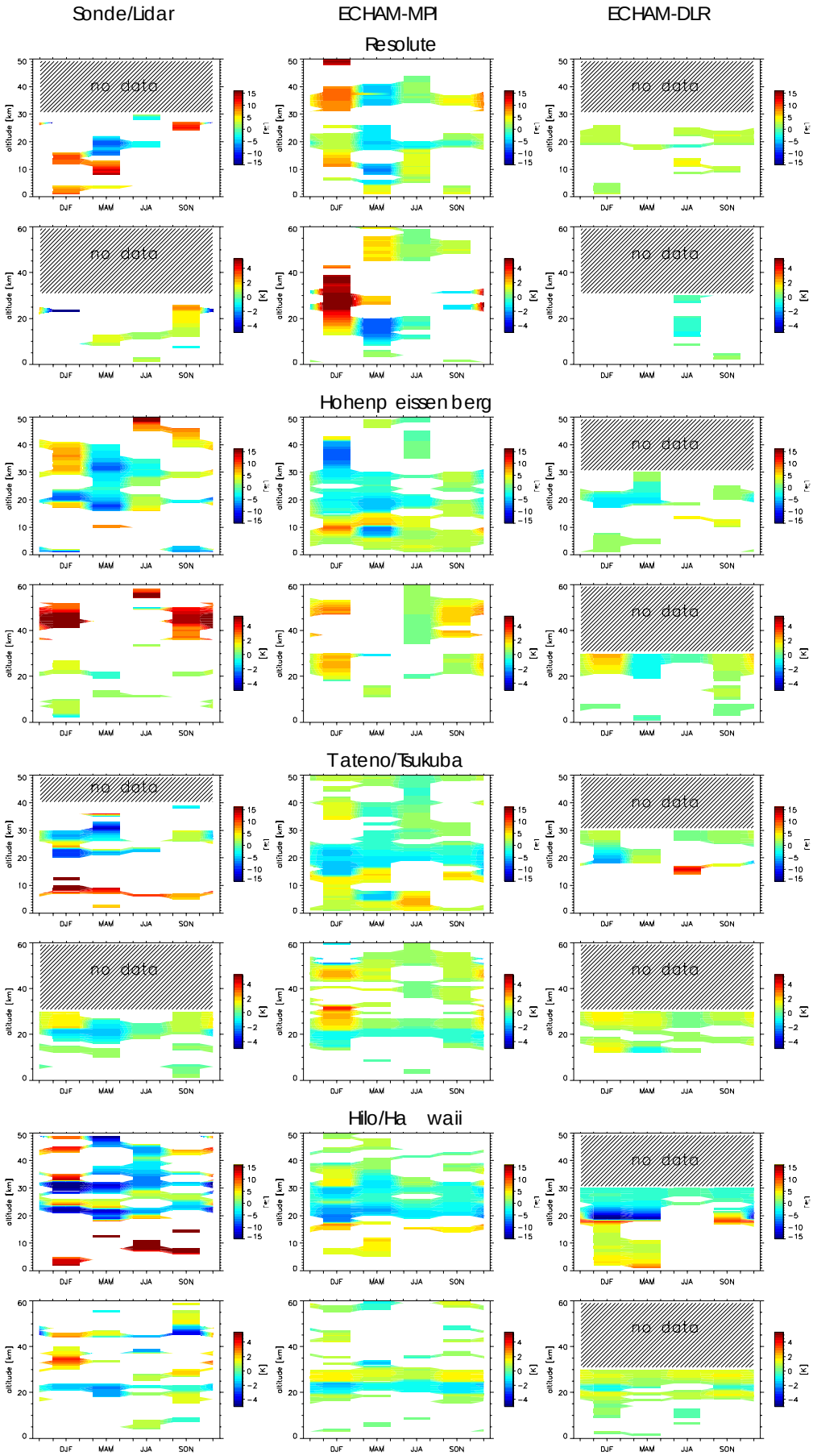

Figure WP1-22: Ozone and temperature fluctuations attributed to the QBO, as measured by 2 standard deviations of QBO related time series terms in Eq. 1. Red colours positive correlation with westerly wind anomalies at 30 hPa, blue colours negative correlation. White regions: no significant QBO influence (90% confidence).

Good agreement between observations and simulations is found for anomalies attributed to zonal wind anomalies at 60°N, 10 hPa in Fig. WP1-25. When the vortex is strong temperature and ozone are low throughout large parts of the stratosphere at Resolute and Hohenpeissenberg, but are high at Tateno and Hilo. At Hohenpeissenberg, upper and lower stratosphere appear to be inversely correlated. The higher ozone values seen in the Hohenpeissenberg observations above 25 km and modelled by ECHAM-MPI above 30 km are probably due to slowing of ozone destroying reactions by the lower temperatures. The higher temperatures seen in Resolute might be due to adiabatic warming by enhanced down-welling in the cold lower vortex.

Given the previously discussed difficulties of obtaining the "right" aerosol signal, the aerosol signal in Fig. WP1-26 is very similar between observations and model simulations. Significantly higher temperatures are found in the lower stratosphere above the lower latitude stations Hilo and Tateno. Ozone in the lower stratosphere is reduced significantly in observations and simulations, at nearly all stations. Ozone in the upper stratosphere is enhanced, both in observations and modelling results. This is due to reduced NO_x, which has been converted to HNO_3 on the volcanically enhanced stratospheric aerosol surface (see contribution DWD, MPI-PROVAM below). As discussed, ECHAM-DLR produces a stratospheric warming after the Pinatubo eruption, different from observations and ECHAM-MPI. Therefore, ECHAM-DLR results at Resolute look different.

Figure WP1-27 shows the size of ozone and temperature variations attributed to ENSO. The most significant results are found for the Pacific stations Hilo and Tateno, where observations and simulations agree very well. For the stratosphere, observations and simulations also agree on generally lower temperatures and lower ozone above Hohenpeissenberg during La-Niña events.

Ozone and temperature in the upper stratosphere are closely coupled through several processes. Low ozone means less solar heating and therefore lower temperatures. This results in a positive correlation between ozone and temperature anomalies. On the other hand the chemical reactions destroying ozone become faster with increasing temperature, resulting in a negative correlation. Above the ozone maximum, enhanced down-welling brings down ozone poor air, but warms the air adiabatically. The opposite is true for up-welling. Vertical motions thus lead to a negative correlation between ozone and temperature anomalies. Meridional transport, on the other hand brings warm and ozone rich air from lower latitudes and leads to positive correlation.

To account for the net effect, temperature anomalies were used as an additional predictor for ozone anomalies in Eq. 1. Only data above 30 km altitude were processed this way. Similarly, ozone anomalies were also used as an additional predictor for temperature. The size and sign of ozone and temperature variations attributed in this way are shown in Fig. WP1-28. Since ECHAM-DLR only provides results below 30 km, it is not included in this figure. For Hilo, both observations and ECHAM-MPI show negative correlation between ozone and temperature variations around 40 km altitude, as well as substantial cross-attributed variations. This is due to the temperature control of chemical ozone destruction. Above Hohenpeissenberg, negative correlation is found in fall, winter and spring, above about 35 km, both in observations and ECHAM-MPI. Since the effect is strongest in winter, vertical motions are a likely cause. Below 35 km, i.e. below the mixing ratio maximum the effect seems to be reversed, both in ECHAM-MPI and in observations. Quite interestingly, the observations at Hohenpeissenberg show a positive correlation in the summer. To a lesser degree this is also seen in the ECHAM-MPI results. Here we might be seeing the effect of ozone heating in the summer.

For Tsukuba and fall/winter/spring, ECHAM-MPI paints a similar picture as for Hohenpeissenberg, whereas results are more complex for Resolute. Unfortunately lidar data for these stations were not available.

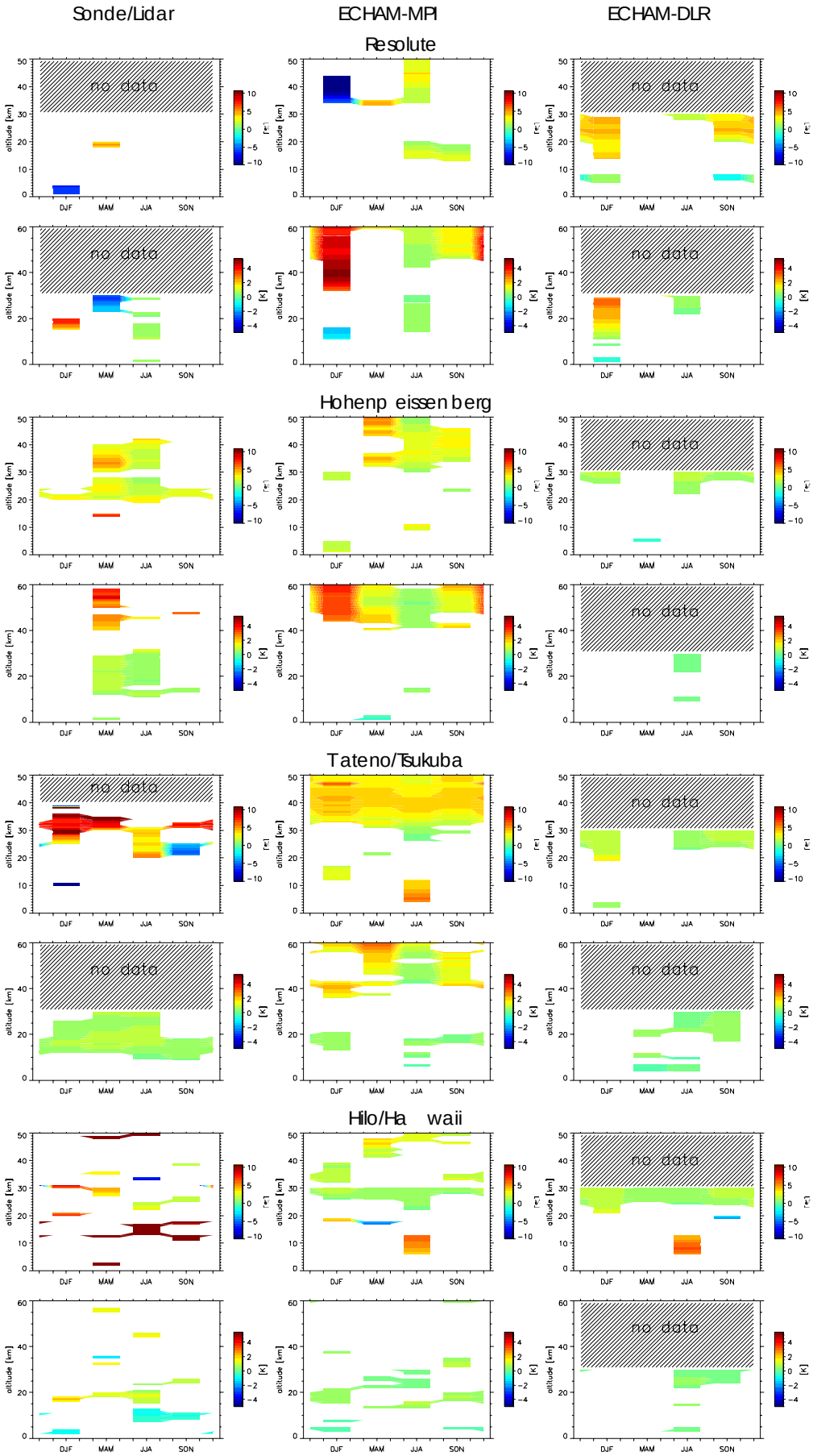

Figure WP1-23: Same as previous figure, but for variations attributed to the 11-year solar-cycle.

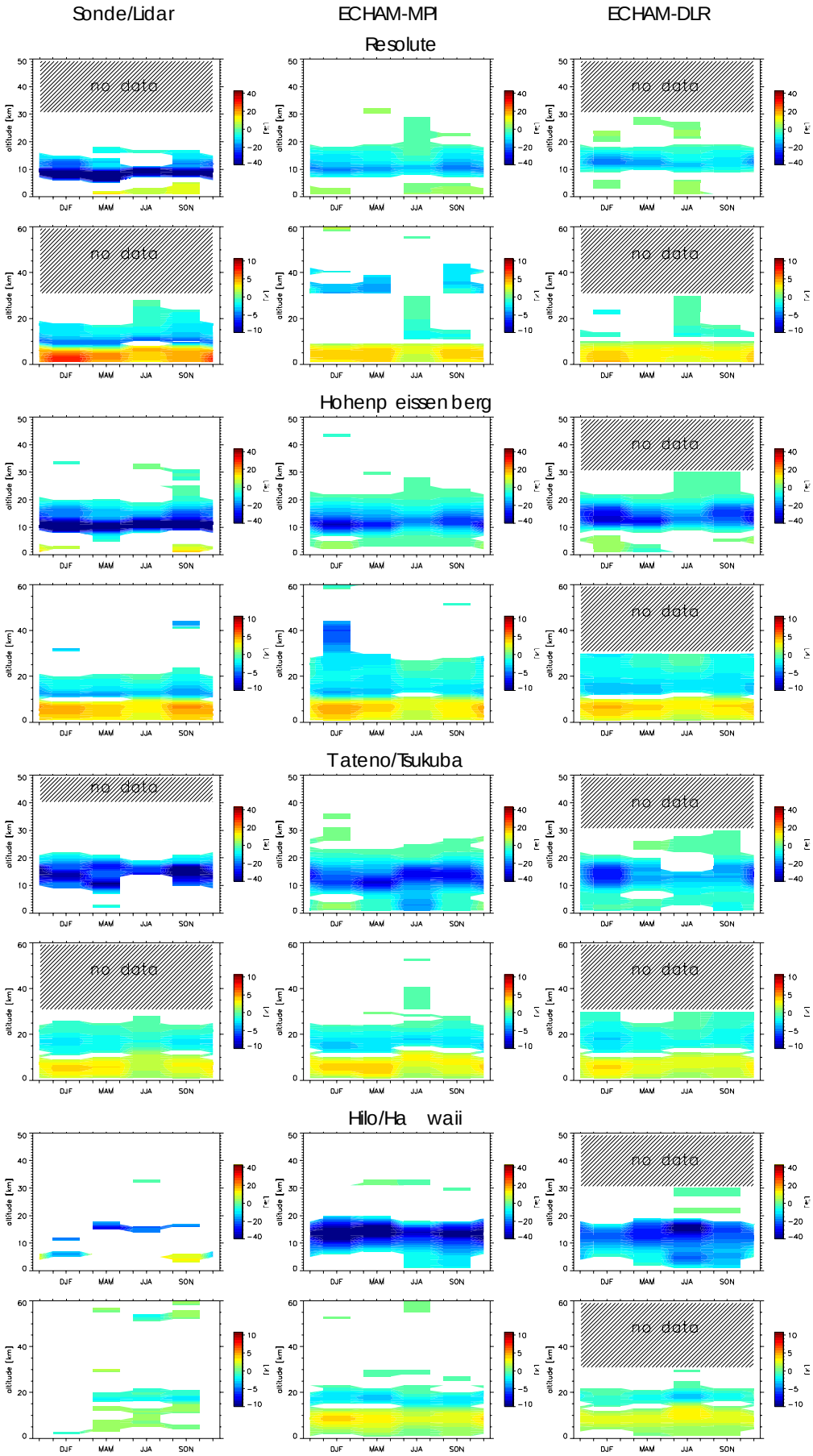

Figure WP1-24: Same as previous figures, but for variations associated with anomalies of tropopause height (for the observations) or tropospheric temperature at 400 hPa (for the ECHAM simulations).

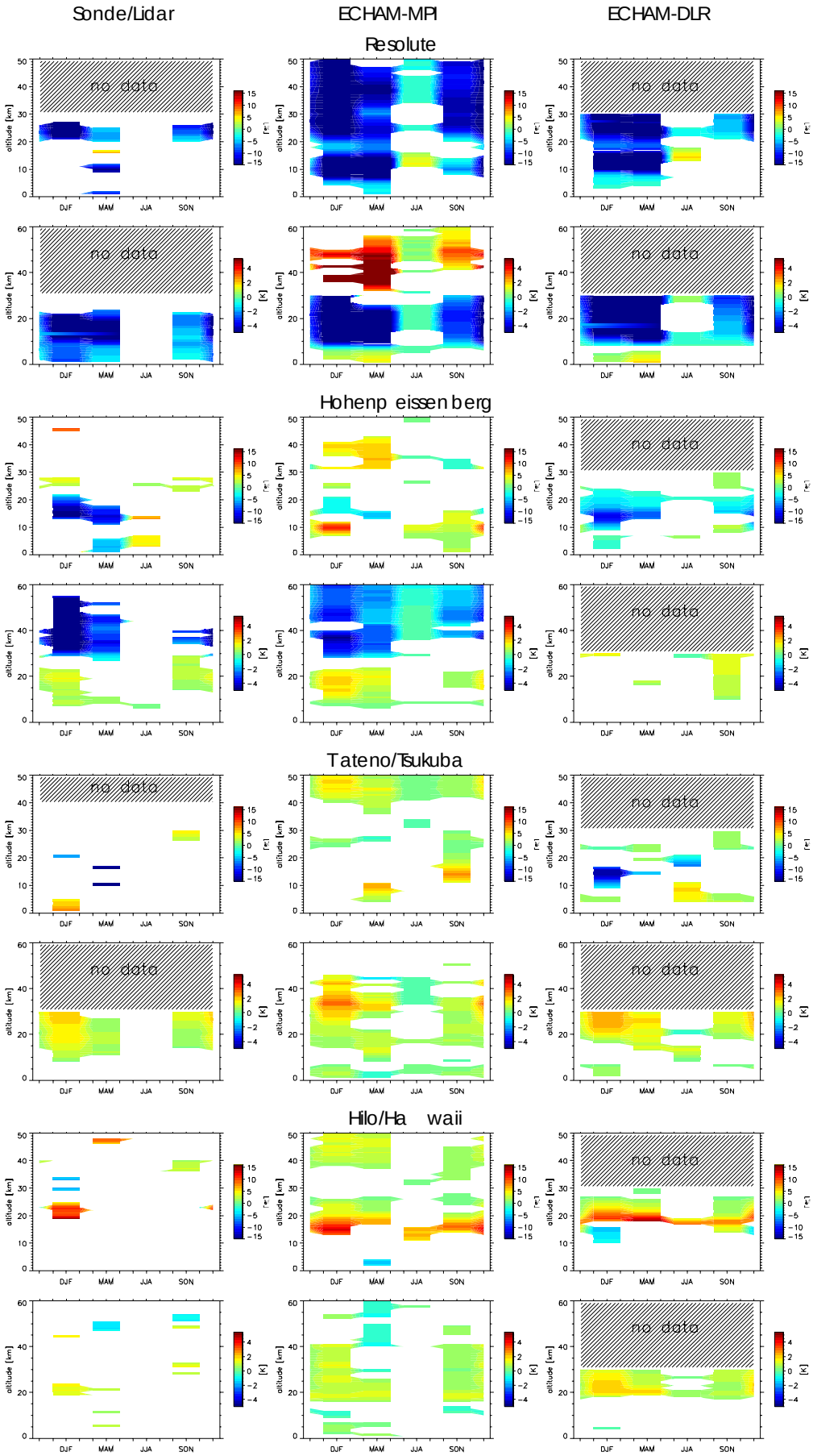

Figure WP1-25: Same as previous figures, but for variations associated with zonal wind anomalies at 60°N, 50 hPa.

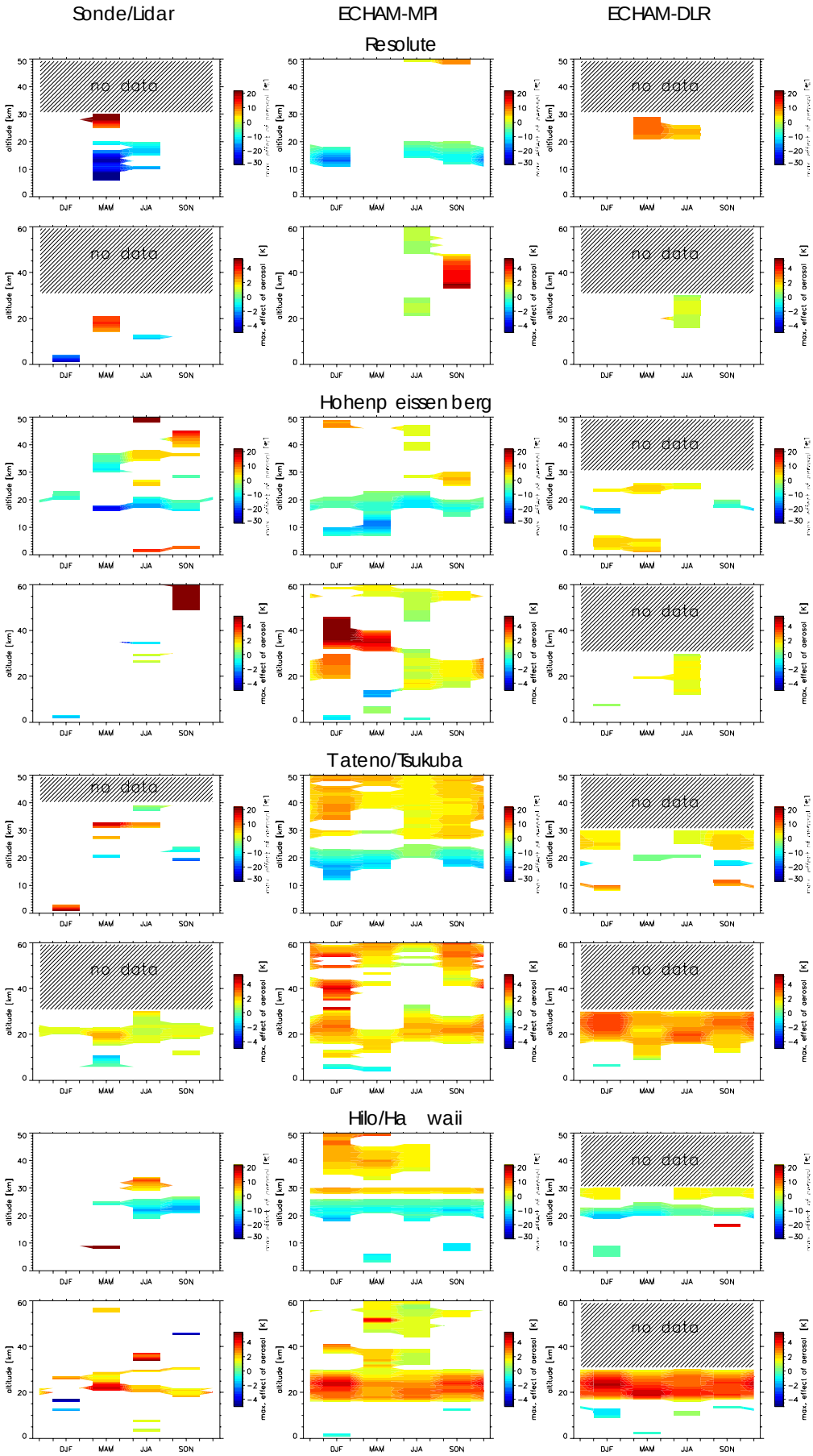

Figure WP1-26: Maximum changes of ozone and temperature attributed to stratospheric volcanic aerosol after the eruption of Mt. Pinatubo in June 1991. White areas: No significant aerosol effect at the 90% confidence level.

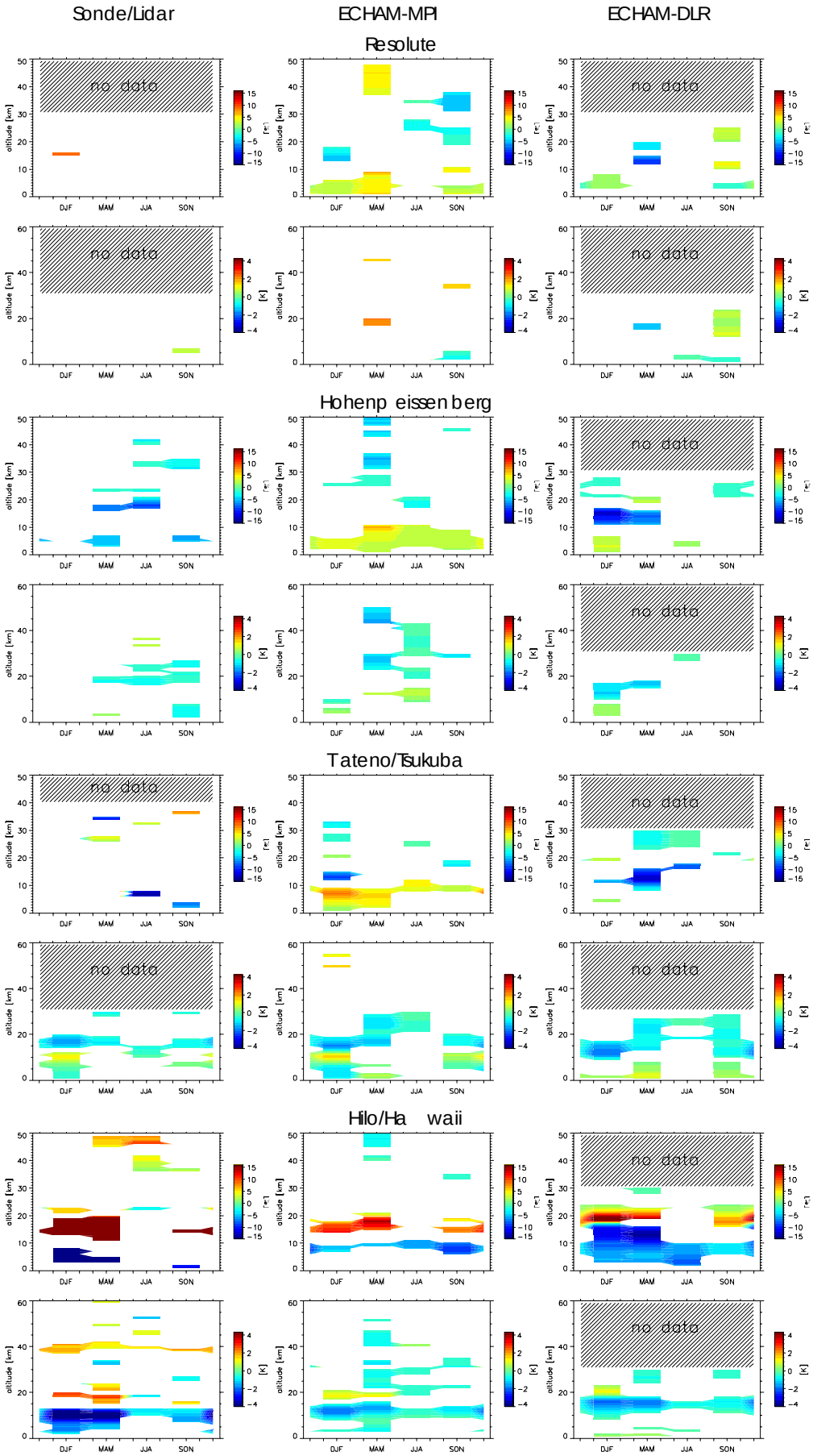

Figure WP1-27: Size (2 standard deviations) of ozone and temperature fluctuations attributed to the Southern Oscillation index. This predictor is positive during La-Niña events and negative during El-Niño events.

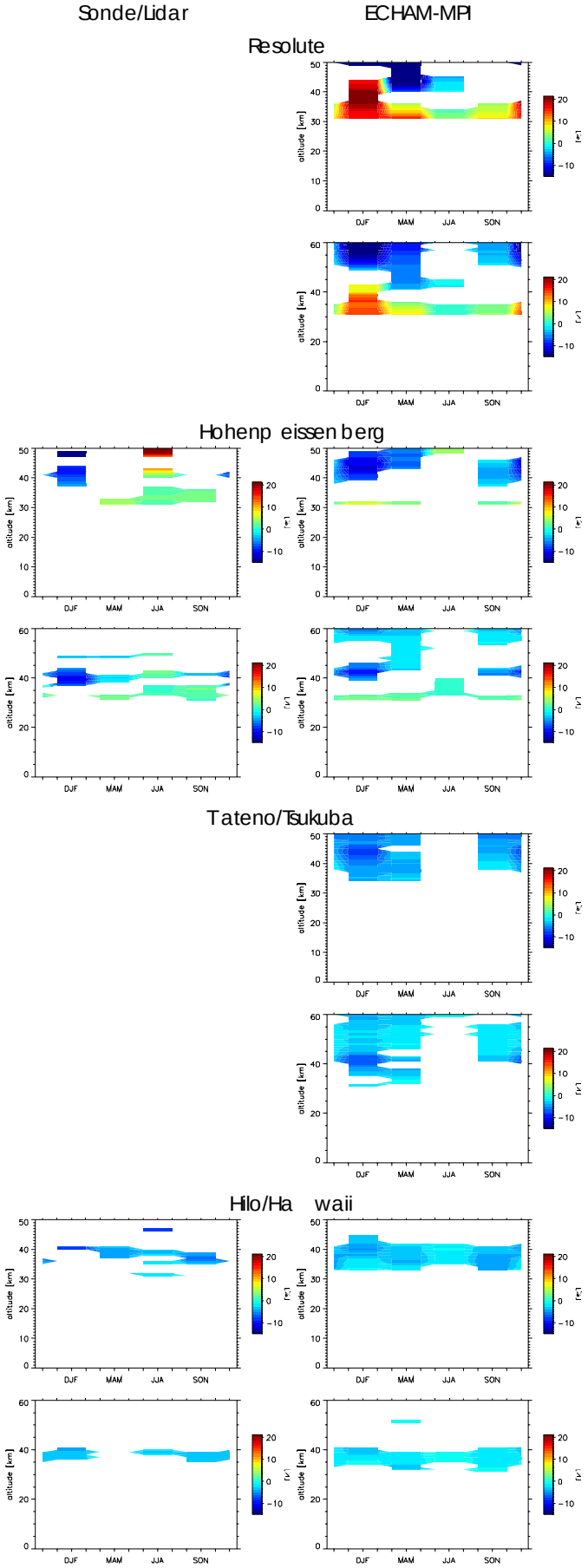

Figure WP1-28: Same as previous figures, but for ozone and the predictor local temperature (upper rows), and for temperature and the predictor ozone (lower rows). Only data above 30 km are processed, therefore no observations are available from Resolute and Tateno, and no results for ECHAM-DLR.

Beginning recovery of upper stratospheric ozone?

The 1987 Montreal Protocol and its amendments have very successfully curbed world-wide emissions of chlorofluorocarbons. As a consequence, the tropospheric chlorine content has maximised a few years ago, and is now starting to decrease. More recently, chlorine in the upper stratosphere also seems to have reached it's maximum and appears to begin decreasing (Anderson et al., 2000). It is a very important question, whether ozone in the upper stratosphere is responding to the declining chlorine, and whether upper stratospheric ozone is starting to increase again. Some recent publications claim that this is the case (Newchurch et al., 2003).

Figure WP1-29 shows ozone anomalies averaged between 35 and 45 km altitude. The data are from the SAGE and HALOE satellite instruments and from ground-based lidars and microwave radiometers. Results from the ECHAM-MPI transient simulation are shown as well. Unfortunately this simulation ends in 1999, because no consistent sea-surface temperature and ice-coverage data set was available after 1999. All data sets, as well as the model simulation agree very well. Upper stratospheric ozone has been declining substantially, and is now between 15 and 25 % lower than around 1980. QBO and 11-year solar cycle very clearly modulate this long-term decline, which is almost entirely caused by anthropogenic chlorine.
The combination of 11-year solar-cycle and long-term trend lead to a stepwise decline, that is most visible above Hawaii.

A particular feature of the stepwise decline is that since about 1996 ozone levels seem to be more or less constant (at Hohenpeissenberg), or even increasing (at Hawaii). It is not unambiguously clear, whether this recent "incline" is due to dropping chlorine concentrations, or whether it is due to the 11-year solar cycle.

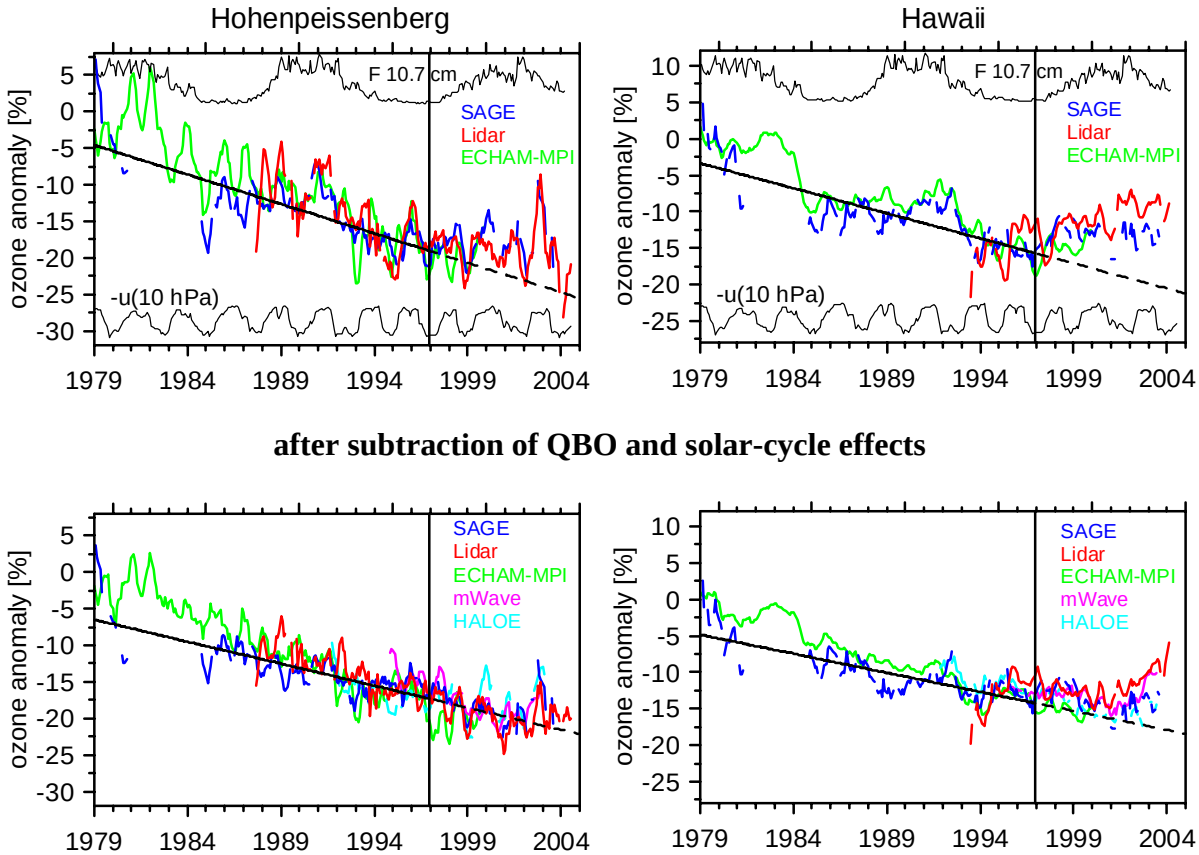

Figure WP1-29: Average ozone anomalies between 35 and 45 km altitude. SAGE (and HALOE) satellite data are zonal means, lidar and microwave data are measured above the station. For Hohenpeissenberg microwave data from Bern (Switzerland) are used. Top panels: Monthly mean anomalies, smoothed by a 5 month running mean. For clarity HALOE and microwave data are omitted. Bottom panels: Same, but after subtracting QBO and solar-cycle effects.

The lower panels of Figure WP1-29 show the ozone anomalies from the upper panels after the subtraction of estimated QBO and solar-cycle effects. Data from additional instruments are shown as well. From the bottom panel it becomes quite clear that the Hohenpeissenberg data show very little evidence for a beginning ozone recovery. At Hawaii, on the other hand, there a fairly clear indication can be seen, that the strong ozone decline of the 1980s has not continued. Ozone levels seem to be increasing again at Hawaii. Two things should be noted:

1. Whether recently higher ozone levels are sign of a beginning recovery or due to the recent maximum of the solar cycle, depends largely on the magnitude of the solar-cycle effect on ozone in recent years. For several reasons, e.g. the two last volcanic erupts occurring near solar maximum, our current estimate of solar cycle effects on ozone is quite uncertain. A beginning recovery should be come clearer towards the end of the beginning solar minimum, i.e. around 2009.
2. Before 2060, upper stratospheric ozone levels are not expected to fully recover to the levels seen around 1980.

Despite these uncertainties, WP1-29 shows some of the first evidence for a beginning recovers of upper stratospheric ozone. As presented in this report, natural variations and their uncertainty are much larger for total ozone that for ozone in the upper stratosphere. Therefore there is no hard evidence for a beginning recover of total ozone at this point. Several more years of high quality measurements, both from ground-based and space-borne instruments, will be needed to document a beginning recovery of the ozone layer and to monitor its future development.

Joint contribution of MPI-MIPS, MPI-C and DWD

Influence of stratospheric aerosol in observed and modelled time series of ozone

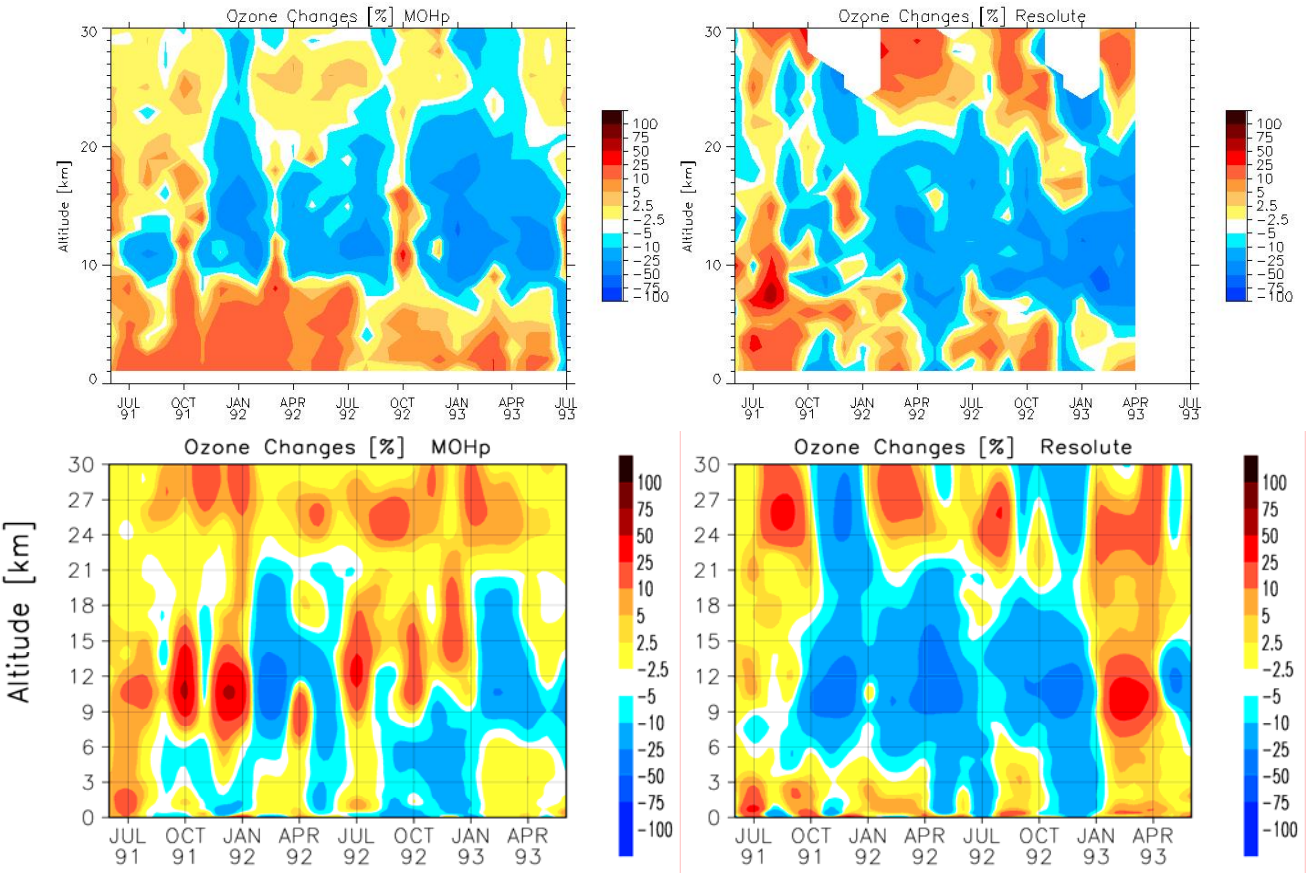

Figure WP1-30: Top: Deviation of ozone monthly means from the climatological mean (1967 to 2002) for the stations Hohenpeissenberg (left) and Resolute (right), for two years after the June 1991 eruption of Mt. Pinatubo. Bottom: Difference between MAECHAM simulation runs with and without volcanic aerosol.

The increase of stratospheric aerosol following the eruption of Mount Pinatubo in June 1991 has led to record low ozone levels and other substantial changes in the atmosphere in the years 1991 to 1993. To investigate these effects, MPI-MIPS and MPI-C have used a separate version of the fully interactive chemistry climate model MAECHAM4(L39), which included a realistic representation of the aerosol cloud and its influence on radiation and chemistry (Timmreck et al., 2003). The difference between model runs with and without volcanic aerosol should give a good estimate for the effect of the Pinatubo eruption on the real atmosphere. The modelled effect can then be compared with actually observed anomalies (see also Figs. WP1-14 and WP1-26). Figure WP1-30 shows such a comparison between modelled aerosol effects and observed ozone anomalies for the stations Hohenpeissenberg and Resolute. As mentioned before, an important caveat is that with both, modelled differences and real data, we are comparing single random samples from many possible evolutions of the modelled or true atmosphere. Early 1993, for example, should not be considered, because the model polar vortex broke down, whereas the real polar vortex did not. Both in model and observations ozone was generally lower throughout the lower stratosphere, between 10 and 22 km altitude. The model calculations show that this ozone depletion is largely caused by increased active chlorine. Active chlorine is increased due to a lack of inactive $ClONO_2$, resulting from decreased NO_x. NO_x is converted to HNO_3 on the volcanic aerosol surface, particularly in the cold lower stratosphere. Above about 22 km slightly enhanced ozone is found, both in model and observations. This enhancement is a direct consequence of decreased NO_x because at these altitudes ozone destruction through NO is reduced. At Resolute in the

Canadian Arctic, agreement between model and observations is best. At mid-latitudes agreement is generally worse. Observations show stronger and longer lasting ozone depletion than the model. Nevertheless, the model replicates the observed ozone changes quite well and provides us with quantitative explanations for their causes.

Joint contribution of MPI-MAECHAM and MPI-C

Changing sources gases and climate change

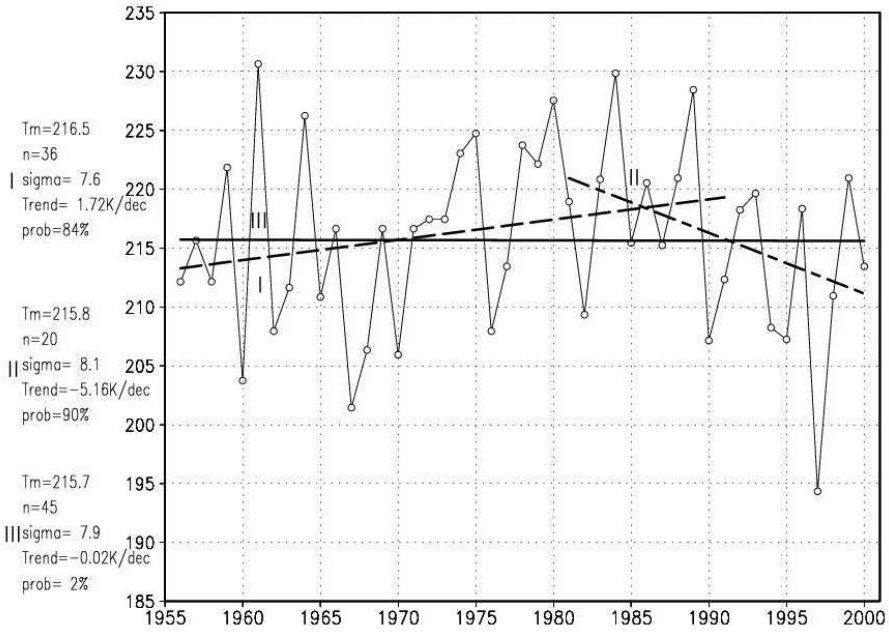

Figure WP1-31: March mean temperature at the North Pole at 30 hPa from the Freie Universität Berlin analyses from 1955 to 2000. Trend I includes data from 1955 to 1991; Trend II from 1981 to 2000; and Trend III from 1955 to 2000; statistical significances are added to the left side.

Changing trace gas concentrations mean changes in the radiative properties of the atmosphere. An important question is, if the substantial change in radiative forcing in the polar stratosphere in the northern hemisphere from 1960s to 2000, due to changes in radiatively active gases like CO_2 or O_3, is strong enough to cause a significant change in polar stratospheric temperature with respect to the high natural variability on intra-seasonal as well as inter-annual time scales. Could the changed composition of the atmosphere explain extremely cold temperatures, for example in 1997 in March (Figure WP1-31)?

This question is addressed on the basis of ECHAM-MPI timeslice experiments that have trace-gas concentrations typical for 1960, 1990 and 2000 (Manzini et al., 2002). Comparison of the 1960 and 2000 scenario experiments shows indeed a significant decrease in polar stratospheric temperature in March and April (Figure WP1-32). MPI-PROVAM, as well as the comparisons presented above, have shown that the MAECHAM4 model is providing a realistic amount of variability in zonal temperature or wind in the North polar stratosphere, a necessary condition for the investigation presented here. Note that the stratospheric polar temperature does not change significantly in the main winter months, and that the March/April cooling is limited in the vertical. This cooling is not related to tropospheric changes in planetary wave activity, a relevant tropospheric parameter. The range of heat fluxes from the troposphere to the stratosphere does not change from the 1960 to the 2000 integration, but the temperature related to a given flux value is decreased by about 5 K (Figure WP1-33). From this it is concluded that the radiative forcing, which is changed by the change in atmospheric composition explains the lowered temperature in March and April in the lower north polar stratosphere. During this late winter cooling the ozone mixing ratio near the North Pole in the lower stratosphere is reduced by about 20%, and the occurrence of PSCs is increased. This positive feedback of radiation and chemistry is, however, limited in time by the late occurrence and also limited in the vertical by a dynamical

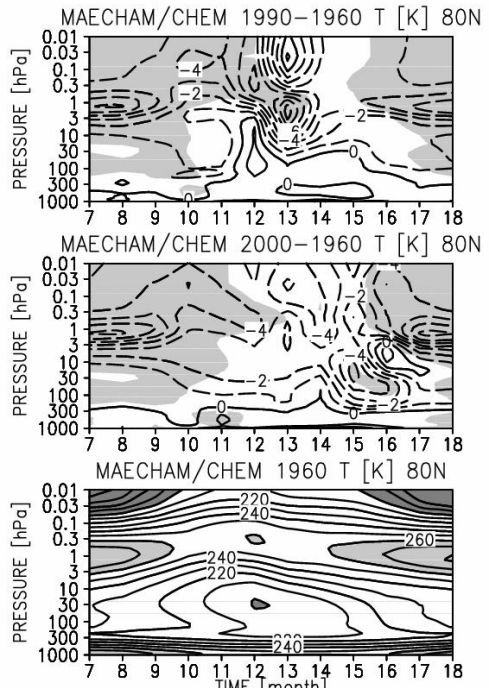

Figure WP1-32: Monthly, zonal mean temperature at 80°N. Difference (top) between the 20-year averages of the 1960 and 1990 simulations, 1990-1960; (middle) between the 20-year averages of the 1960 and 2000 simulations, 2000-1960. Contour: 1 K, light shade indicates a statistically significant difference at 95%, t-test. (Bottom) 20-year averages from the 1960 simulation. Contour: 10 K, light shade > 260 K, dark shade < 200 K. The time axis runs from July (month=7) to June (month=18).

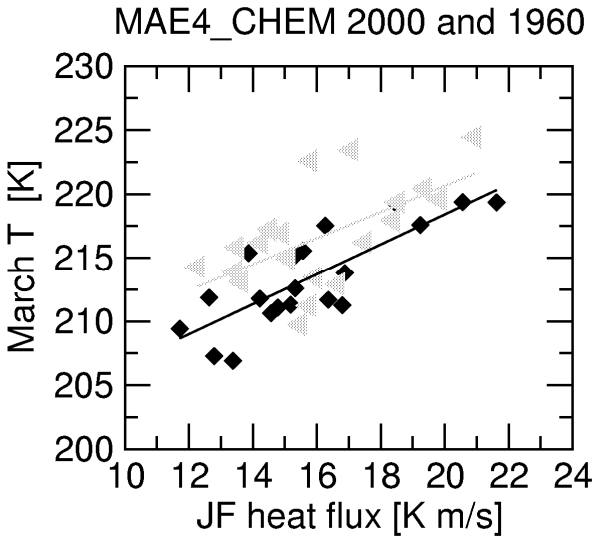

Figure WP1-33: Scatter plot of (left) January-February meridional heat flux at 100 hPa (40N-80N area-weighted average) and March temperature at 50 hPa (60°N-90°N area weighted average). Each symbol is a mean from an individual year. Grey is for the 1960 simulation and black for the 2000 simulation.

feedback initiated first in the mesosphere by a changed gravity wave forcing, a novel mechanism found in this work. Hence the natural variability in the winter circulation of the North polar stratosphere is high enough to mask radiative-chemical feedback effects in most winter months, except for the late winter months of March and April.

Contribution of MPI-C

Solar forcing on the troposphere via the stratosphere

Apart from the transient runs, the atmospheric response to the 11-year solar cycle was also studied using the fully interactive 3D coupled chemistry-general circulation model with a complete seasonal cycle MAECHAM/CHEM based on two 20 year timeslice experiments for solar maximum and solar minimum radiation conditions (Tourpali et al., 2003). The stratosphere-troposphere system shows significant responses to a realistic solar cycle enhancement of UV-radiation at solar maximum. This response consists of increases in stratospheric ozone and temperature, giving rise to changes in the zonal wind from the stratosphere into the troposphere. Computed changes of stratospheric ozone, temperature and zonal wind are generally in agreement with observed changes between solar minimum and solar maximum (see also discussion of Figs. WP1-10 and WP1-16). Observed pattern changes of the stratospheric response between early and late winter are approximately reproduced by the model. Our radiative forcing results show that the 11-year solar cycle effect on global mean temperature is negligible, but simulated responses of sea level pressure do suggest that regional effects are probably significant, e.g. by affecting the North Atlantic Oscillation.

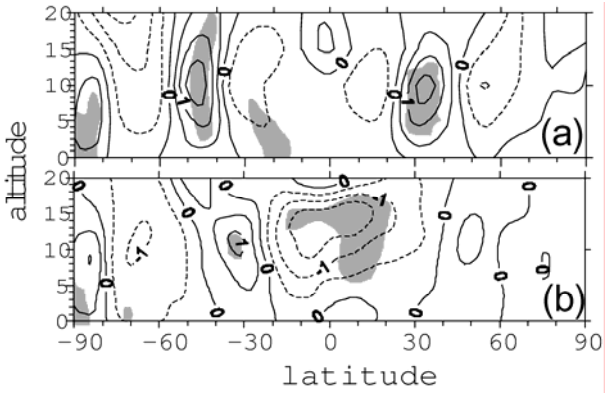

Figure WP1-34: Tropospheric zonal wind differences (m/sec) for solar maximum relative to solar minimum for (a) January and (b) July. Shading indicates the 95% significance level.

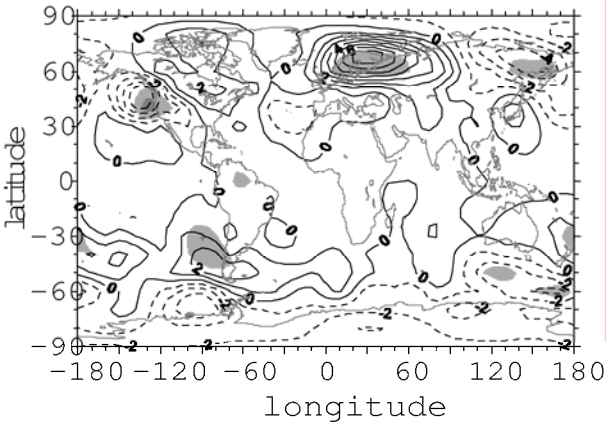

Figure WP1-35: Mean sea level pressure change (hPa) from solar min. to solar max. in January. Shading indicates the 95% significance level.

In the troposphere (Figure WP1-34), the tropics show a decrease of westerlies (increase of easterlies) at solar maximum, in January as well as in July. Moving polewards we see an increase of the westerlies, followed again by a decrease at still higher latitudes and so on. This banded structure of the tropospheric response was found also in the studies by Haigh (1999). In fact, the results for individual months show that this banded structure moves more or less north and southward with the sun. For all months we find certain latitude-height positions where the zonal mean changes are statistically significant at the 95% level (compare Fig. WP1-16). This indicates that the solar effect is likely real and its magnitude is sufficiently large to exceed natural variability over 20 years. For the northern hemisphere mid latitudes, this alternating pattern means a decrease of the zonal mean westerlies in winter and an increase in summer. For the southern hemisphere we find a larger response in January (Figure WP1-34a) than in July (Figure WP1-34b). Nevertheless, from Fig. WP1-35, which shows the computed changes of mean sea level pressure for January as a representative winter month, we infer that the idea of regional climate responses to solar activity is not completely unrealistic. What we see in Figure WP1-21 is that the pressure gradient over the North Atlantic is decreased, which would mean a lowering of the NAO (North Atlantic Oscillation)-index. According to Hurrell and van Loon (1997) this would favour lower temperatures in Western Europe. This is clearly in line with the decrease of January and winter mean temperature in the lower layers of the atmosphere at mid- high latitudes of the northern hemisphere, which we find in our computations. The above results are also in line with recent work by Kodera (2002) on the NAO modulation by the solar cycle. The lower sea level pressure in the polar southern hemisphere occurs in each month in the season (marginally significant in the zonal mean). As the sea surface temperature is kept constant in our model runs, except for the seasonal cycle, we have to be careful not to draw firm conclusions regarding the pressure and temperature changes near the surface. Considering the above, we may conclude that realistic changes of the solar UV-radiation influence the stratosphere- troposphere system in a significant way. The pattern of the tropospheric response shows an increase of the tropical easterlies in all seasons, as well as significant changes of the zonal mean westerlies at the temperate latitudes, especially in northern winter. These circulation changes will give rise to regional changes of weather and climate, although the precise nature and sign of these changes have to be further investigated.

However, the results of the experiment certainly add to the credibility of the recent claim by Baldwin and Dunkerton (1999) that stratospheric processes may act as a precursor of anomalous weather regimes. Enhanced UV and partly also the enhanced radiation in the visible part of the spectrum are absorbed in the stratosphere. This results in changes of ozone and temperature, which in turn will give rise to changes of the radiative forcing of the troposphere which are small and probably too small to cause the calculated tropospheric effects. Analysis of the wave structure and amplitudes of our response patterns has shown that at solar maximum in the troposphere wave number 1 is favoured at the cost of wave numbers 2 and 3 as suggested by Kodera (1995). In the upper stratosphere wave number

1 appears to be the dominant wave component under solar maximum as well as under solar minimum conditions, although in our experiment it appears to be weaker at solar maximum.

New Publications with contributions from WP1

Austin J., D. Shindell, S. R. Beagley, C. Brühl, M. Dameris, E. Manzini, T. Nagashima, P. Newman, S. Pawson, G. Pitari, E. Rozanov, C. Schnadt, and T. G. Shepherd (2003): Uncertainties and assessments of chemistry-climate models of the stratosphere, *Atmos. Chem. Phys.*, **3,** 1-27, 2003.

Horinouchi, T, S. Pawson, K. Shibata, U. Langematz, E. Manzini, M. A. Giorgetta, F. Sassi, R. J. Wilson, K. Hamilton, J. de Granpre, A. A. Scaife, Tropical cumulus convection and upward propagating waves in middle atmospheric GCMs, *J. Atmos. Sci.,* **60,** 2765-2782, 2003.

Manzini, E., B. Steil, C. Brühl, M. A. Giorgetta and K. Krüger. A new interactive chemistry-climate model. II: Sensitivity of the middle atmosphere to ozone depletion and increase in greenhouse gases: Implications for recent stratospheric cooling, *J. Geophys. Res*., **108(**D14), 4429, doi:10.1029/2002JD002977, 2003.

Steil, B., C. Brühl, E. Manzini, P.J. Crutzen, J. Lelieveld, P.J Rasch, E. Roeckner, K. Krüger. A new interactive chemistry climate model. I: Present day climatology and interannual variability of the middle atmosphere using the model and 9 years of HALOE/UARS data, *J. Geophys. Res*., **108**(D9), 4290, doi:10.1029/2002JD002971, 2003.

Steinbrecht, W., Haßler, B., Claude, H., Winkler, P., Stolarski, R.S.: Global distribution of total ozone and lower stratospheric temperature variations. *Atmos. Chem. Phys*., 3, 1421-1438, 2003.

Steinbrecht, W., Claude, H., Winkler, P.: Enhanced Upper Stratospheric Ozone: Sign of Recovery or Solar Cycle Effect? *J. Geophys. Res.*, 109(D2), D02308, doi:10.1029/2003JD004284, 2004a.

Steinbrecht, W., H. Claude, and P. Winkler. Reply to comment by D. M. Cunnold et al. on ‘‘Enhanced upper stratospheric ozone: Sign of recovery or solar cycle effect?,’’ *J. Geophys. Res.,* 109, D14306, doi:10.1029/2004JD004948, 2004b.

Timmreck, C., H.-F. Graf and B. Steil, Aerosol chemistry interactions after the Mt. Pinatubo eruption, in *Volcanism and the Earth's Atmosphere,* eds. A. Robock and C. Oppenheimer, AGU Monograph, 139, p 213-225, 2003.

Tourpali, K., Schuurmans, C.J.E., van Dorland, R., Steil, B., and Brühl, C., Stratospheric and tropospheric response to enhanced solar UV-radiation: A model study, *Geophys. Res. Lett.*, 30, doi: 10.1029/2002GL016650, 2003.

References

Anderson, J., J.M. Russell, S. Solomon, and L.E. Deaver, HALOE confirmation of stratospheric chlorine decreases in accordance with the Montreal protocol, *J. Geophys. Res.*, 105, 4483-4490, 2000.

Baldwin, M.P., and Dunkerton, T.J., Propagation of the Arctic Oscillation from the stratosphere to the troposphere, *J. Geophys. Res.,* 104, 30,937-30,946, 1999.

Baldwin, M.P., Gray, L.J., Dunkerton, T.J., Hamilton, K., Haynes, P.H., Randel, W.J., Holton, J.R., Alexander, M.J., Hirota, I., Horinouchi, T., Jones, D.B.A., Kinnersley, J.S., Marquardt, C., and Takahashi, M., The Quasi-Biennial Oscillation, *Rev. Geophys.*, 39, 179-229, 2001.

Coughlin, K, and K.-K. Tung, QBO Signal found at the Extratropical Surface through Northern Annular Modes, *Geophys. Res. Lett.*, 28, 4563-4566, 2001

Fioletev, V.E., Bodeker, G.E., Miller, A.J., McPeters, R.D., and Stolarski, R., Global and zonal total ozone variations estimated from ground-based and satellite measurements: 1964-2000, *J. Geophys. Res.*, 107, 4647, doi:10.1029/2001JD001350, 2002.

Haigh, J.D. A GCM study of climate change in response to the 11- year solar cycle, *Quart. J. R .Met .Soc.*, 125, 871- 892, 1999.

Hein, R. et al., Results of an interactively coupled atmospheric chemistry-general circulation model: Comparison with observations. *Ann. Geophys*., 19, 435-457, 2001.

Hurrell, J.W. and H. van Loon. Decadal variations in climate associated with the North Atlantic Oscillation, *Climatic Change*, 36, 301- 326, 1997.

Kistler, R., Kalnay, E., Collins, W., Saha, S., White, G., Woollen, J., Chelliah, M., Ebisuzaki, W., Kanamitsu, M., Kousky, V., van den Dool, H., Jenne, R., and Fiorino, M., The NCEP-NCAR 50-Year Reanalysis: Monthly Means, CD-ROM and Documentation, *Bull. Am. Met. Soc.*, 82, 247-267, or http://wesley.wwb.noaa.gov/reanalysis.html, 2001.

Koch, G., H. Wernli, J. Staehelin and T. Peter, Reply to comment by H. Teitelbaum et al. on "A Lagrangian analysis of stratospheric ozone variability and long-term trends above Payerne (Switzerland) during 1970-2001" , *J. Geophys. Res.,* 108, 4675, doi:10.1029/2003JD003911, 2003.

Kodera, K., On the origin and nature of the interannual variability of the winter stratospheric circulation in the northern hemisphere, *J. Geophys. Res.*, 100, 1995.

Kodera, K., Solar cycle modulation of the North Atlantic Oscillation: Implication in the spatial structure of the NAO, *Geophys. Res. Lett.*, 29, 8, 59, 2002.

Labitzke, K., and van Loon, H., *The stratosphere: phenomena, history, and relevance*, Springer Verlag, Berlin, 197 pg., 1999.

Newchurch, M.J., Yang, E., Cunnold, D.M., Reinsel, G.C., Zawodny, J.M., Russell III, J.M.: Evidence for Slowdown in Stratospheric Ozone Loss: First Stage of Ozone Recovery. *J. Geophys. Res.*, 108(D16), 4507, doi:10.1029/2003JD003471, 2003.

Perlwitz, J., and H.-F. Graf. The statistical connection between tropospheric and stratospheric circulation of the Northern Hemisphere in winter . *J. Clim.,* 8, 2281-2295, 1995.

Ramaswamy, V., Chanin, M.L., Angell, J., Barnett, J., Gaffen, D., Gelman, M., Keckhut, P., Koshelkov, Y., Labitzke, K., Lin, J.J.R., O`Neil, A., Nash, J., Randel, W., Rood, R., Shiotani, M., Swinbank, R., and Shine, K., Stratospheric temperature trends: observations and model simulations, *Rev. Geophys.,* 39, 71-122, 2001.

Rex, M., R. J. Salawitch, P. von der Gathen, N. R. P. Harris, M. P. Chipperfield, and B. Naujokat, Arctic ozone loss and climate change, *Geophys. Res. Lett.*, 31, L04116, doi:10.1029/2003GL018844, 2004.

Shine, K. P., M. S. Bourqui, P.M. De F. Forster, S. H. E. Hare, U. Langematz, P. Braesicke, V. Grewe, M. Ponater, C. Schnadt, C. A. Smith, J. D. Haigh, J. Austin, N. Butchart, D. T. Shindell, W. J. Randel, T. Nagashima, R. W. Portmann, S. Solomon, D. J. Seidel, J. Lanzante, S. Klein, V. Ramaswamy, M. D. Schwarzkopf, A comparison of model-simulated trends in stratospheric temperatures. *Q. J. Roy. Met Soc.*, 129, 590, 1565-1588, 2003.

Stolarski, R.S. and Hollandsworth Frith, S., Combined total ozone record from TOMS and SBUV instruments, http://code916.gsfc.nasa.gov/Data_services/merged/mod_data.public.html, 2003.

WMO (World Meteorological Organization), Scientific Assessment of Ozone Depletion: 2002, Global Ozone Research and Monitoring Project-Report No. 47, 498 pp., Geneva, http://www.wmo.ch/web/arep/ozone.html, 2003.